STABILITY OF MONAZITE AND DISTURBANCE OF THE Th-U-Pb SYSTEM UNDER EXPERIMENTAL CONDITIONS OF 250–350 °C AND 200–400 MPa

Bartosz BUDZYŃ[1, 2], Patrik KONEČNÝ[3] & Gabriela A. KOZUB-BUDZYŃ[4]

[1] *Institute of Geological Sciences, Polish Academy of Sciences, Research Centre in Kraków ING PAN, Senacka 1, PL-31002 Kraków, Poland; e-mail: ndbudzyn@cyf-kr.edu.pl*
[2] *Institute of Geological Sciences, Jagiellonian University, Oleandry 2a, PL-30063 Kraków, Poland*
[3] *Dionýz Štúr State Geological Institute, Mlynská dolina 1, SK-81704 Bratislava, Slovak Republic; e-mail: patrik.konecny@geology.sk*
[4] *AGH University of Science and Technology, Faculty of Geology, Geophysics and Environmental Protection, Mickiewicza 30, PL-30059 Krakow, Poland; e-mail: lato@agh.edu.pl*

Abstract: This experimental study provides important data filling the gap in our knowledge on monazite stability under conditions of fluid-mediated low-temperature metamorphic alteration and post-magmatic hydrothermal alterations. The stability of monazite and maintenance of original Th-U-total Pb ages were tested experimentally under P-T conditions of 250–350 °C and 200–400 MPa over 20–40 days. The starting materials included the Burnet monazite + K-feldspar ± albite ± labradorite + muscovite + biotite + SiO_2 + CaF_2 and 2M $Ca(OH)_2$ or $Na_2Si_2O_5$ + H_2O fluid. In the runs with 2M $Ca(OH)_2$, monazite was unaltered. REE-enriched apatite formed at 350 °C and 400 MPa. The presence of the $Na_2Si_2O_5$ + H_2O fluid promoted the strong alteration of monazite, the formation of secondary REE-enriched apatite to fluorcalciobritholite, and the formation of REE-rich steacyite. Monazite alteration included the newly developed porosity, patchy zoning, and partial replacement by REE-rich steacyite. The unaltered domains of monazite maintained the composition of the Burnet monazite and its age of (or close to) ca. 1072 Ma, while the altered domains showed random dates in the intervals of 375–771 Ma (250 °C, 200 MPa run), 82–253 Ma (350 °C, 200 MPa), and 95–635 Ma (350 °C, 400 MPa). The compositional alteration and disturbance of the Th-U-Pb system resulted from fluid-mediated coupled dissolution-reprecipitation. In nature, such age disturbance in monazite can be attributed to post-magmatic alteration in granitic rocks or to metasomatic alteration during metamorphism. Recognition of potentially altered domains (dark patches in high-contrast BSE-imaging, developed porosity or inclusions of secondary minerals) is crucial to the application of Th-U-Pb geochronology.

Key words: Monazite, apatite, steacyite, rare earth elements, geochronology, experimental petrology.

INTRODUCTION

Monazite ($REEPO_4$) is one of the main hosts of rare earth elements (REE) and actinides in the Earth's crust. The stability of monazite, strongly dependent on temperature, pressure, and composition of host rock and fluid, has been widely studied in terms of alteration and replacement by apatite, allanite and epidote, recognized in igneous rocks affected by a fluid-mediated overprint (e.g., Broska and Siman, 1998; Broska *et al.*, 2005), and amphibolite-facies metamorphic rocks (e.g., Finger *et al.*, 1998; Majka and Budzyń, 2006; Janots *et al.*, 2008; Budzyń *et al.*, 2010; Ondrejka *et al.*, 2012). It has been known for half a century

that monazite may be stable in Ca-poor granitic rocks (bulk composition of <0.7 wt % CaO) and that allanite is present in Ca-rich granites (>1.8 wt % CaO), while both monazite and allanite are stable in intermediate granites with 0.7–1.8 wt % CaO bulk content (Lee and Dodge, 1964; Lee and Bastron, 1967). The stability relationships between monazite and allanite under upper greenschist- to amphibolite-facies conditions were constrained *via* thermodynamic modelling (Janots *et al.*, 2007; Spear, 2010). There are also experimental data, which replicate the mineral composition of the whole rock to determine the relative stabilities of monazite,

allanite, and apatite under upper greenschist- to amphibolite-facies conditions (Budzyń *et al.*, 2011), and recently expanded to a wide P-T range of 450–750 °C and 2–10 kbar (Budzyń *et al.*, 2014). However, there are limited data on monazite stability during low-temperature hydrothermal and diagenetic processes (Poitrasson *et al.*, 1996, 2000; Cuney and Mathieu, 2000; Hecht and Cuney, 2000; Read *et al.*, 2002; Rasmussen and Muhling, 2007, 2009).

The incorporation of Th and U in monazite offers the potential for Th-U-Pb dating (Parrish, 1990). Because of the negligible content of common Pb relative to radiogenic Pb, a monazite age can be constrained by "chemical" Th-U-total Pb dating using the electron microprobe (Suzuki and Adachi, 1991; Montel *et al.*, 1996; Konečný *et al.*, 2004; Jercinovic and Williams, 2005; Pyle *et al.*, 2005; Williams *et al.*, 2007; Jercinovic *et al.*, 2008; Suzuki and Kato, 2008; Spear *et al.*, 2009). Electron microprobe microanalysis is a powerful tool to link monazite ages with textural content and put absolute time constraints on metamorphic, metasomatic or deformational processes, constrain rates of these processes, and finally, to put absolute time constraints on the reconstruction of pressure-temperature-deformation paths (Williams and Jercinovic, 2002; Williams *et al.*, 2007). Because of these considerations, monazite became one of the most commonly used geochronometers in the last two decades. Monazite is characterized by high diffusional closure temperature of 800–900 °C, with respect to Th and Pb (Cherniak *et al.*, 2004; Gardes *et al.*, 2006; Cherniak and Pyle, 2008). However, an age disturbance was recognized typically in monazite revealing patchy zoning, related to fluid-aided coupled dissolution-reprecipitation during post-magmatic, metasomatic or hydrothermal alteration in granitic (Townsend *et al.*, 2000; Petrík and Konečný, 2009; Appel *et al.*, 2011; Tartèse *et al.*, 2011; Ayers *et al.*, 2013; Lisowiec *et al.*, 2013) and metamorphic rocks (Aleinikoff *et al.*, 2012). Knowledge about the advantages and limitations of using monazite as a geochronometer expanded significantly during the last decade with respect to possible disturbance of the Th-U-Pb system. Experimental studies shown that alteration of monazite related to the fluid-mediated coupled dissolution-reprecipitation process may significantly disturb Th-U-Pb system (Teufel and Heinrich, 1997; Seudoux-Guillaume *et al.*, 2002a; Harlov *et al.*, 2007, 2011; Harlov and Hetherington 2010; Hetherington *et al.*, 2010; Budzyń *et al.*, 2011), leading to resetting of the monazite clock, even far below the diffusional closure temperature, that is at 450 °C and 450 MPa (Williams *et al.*, 2011).

The aim of this study was to experimentally explore and constrain the stability of monazite under conditions of 250–350 °C and 200–400 MPa, in the presence of two of the most aggressive fluids, previously used by Budzyń *et al.* (2011). The innovation of this work lies in utilizing a mineral assemblage that roughly replicates the composition of granitic rocks. The new experimental data provide petrological implications for applications of monazite in reconstructing low-grade metamorphic processes. Further geochronological implications are related to the experimental disturbance of the Th-U-Pb system in monazite, significantly modifying the original age.

ANALYTICAL AND EXPERIMENTAL METHODS

Analytical methods

The starting minerals and experimental products were evaluated using a Hitachi S-4700 field emission scanning electron microscope (FESEM), equipped with an energy dispersive spectrometer (EDS), at the Institute of Geological Sciences, Jagiellonian University (Kraków, Poland).

The chemical analyzes of minerals were performed using a Cameca SX 100 electron microprobe equipped with a four-wavelength spectrometer, at the Department of Special Laboratories, Laboratory of Electron Microanalysis, Geological Institute of Dionýz Štúr (Bratislava, Slovak Republic). The monazite was analyzed using a 15 kV accelerating voltage, a 180 nA beam current, and a 3-µm beam size focused on the grain mount, coated with ca. 25 nm carbon film. The following natural and synthetic standards, and corresponding spectral lines were used: apatite (P Kα), $PbCO_3$ (Pb Mα), ThO_2 (Th Mα), UO_2 (U Mβ), YPO_4 (Y Lα), $LaPO_4$ (La Lα), $CePO_4$ (Ce Lα), $PrPO_4$ (Pr Lβ), $NdPO_4$ (Nd Lα), $SmPO_4$ (Sm Lα), $EuPO_4$ (Eu Lβ), $GdPO_4$ (Gd Lα), $TbPO_4$ (Tb Lα), $DyPO_4$ (Dy Lβ), $HoPO_4$ (Ho Lβ), $ErPO_4$ (Er Lβ), $TmPO_4$ (Tm Lα), $YbPO_4$ (Yb Lα), $LuPO_4$ (Lu Lβ), fayalite (Fe Kα), barite (S Kα), wollastonite (Ca Kα, Si Kα), $SrTiO_3$ (Sr Lα), Al_2O_3 (Al Kα), GaAs (As Lα). The counting times on peak/background (in sec.) were as follows: P 10/10, Pb 300/150, Th 35/17.5, U 80/80, Y 40/20, La 5/5, Ce 5/5, Pr 15/15, Nd 5/5, Sm 5/5, Eu 25/25, Gd 10/10, Tb 7/7, Dy 35/35, Ho 30/30, Er 50/50, Tm 15/15, Yb 15/15, Lu 100/100, Fe 5/5, S 10/10, Ca 10/10, Sr 20/20, Al 10/10, Si 10/10, As 120/120. The monazite concentrations were recalculated using age equations from Montel *et al.* (1996) and evaluated using in-house DAMON software (P. Konečný, unpublished). Additional analytical information can be found in Konečný *et al.* (2004), Petrík and Konečný (2009) and Vozárová *et al.* (2014). Apatite, fluorcalciobritholite and REE-rich steacyite were analyzed using two conditions, automatically switched during a run from (1) 15 kV, 20 nA for F (30/15 sec), Si (10/5), Na (10/5), Al (10/5), Mg (10/5) P (10/5), Ca (10/5), K (10/5), Cl (10/5), Fe (10/5), Mn (10/5), Ti (10/5); to (2) 15 kV, 80 nA for Y (30/15), Sr (60/30), Pb (30/15), Ce (40/20), La (40/20), Nd (30/15), Pr (50/25), Sm (30/15), Eu (60/30), Gd (40/20), Tb (20/10), Dy (60/30), Th (30/15), U (40/20), and a 1–5 µm beam size, depending on the size of the grain analyzed. Silicate minerals were analyzed using 15 kV accelerating voltage, 20 nA current, and beam size of 5 µm for biotite, K-feldspar, and 10 µm for muscovite, albite and labradorite. The counting times were 10 sec. on peak and 5 sec. on background for each element.

Additional analyses of silicates and compositional X-ray maps of altered monazite were performed using a JEOL SuperProbe JXA-8230 electron microprobe at the Laboratory of Critical Elements AGH-KGHM, Faculty of Geology, Geophysics and Environmental Protection, AGH University of Science and Technology (Kraków, Poland). The silicates were analyzed using a 15 kV accelerating voltage, 20 nA beam current, and focused beam to 5 µm beam size. The counting times on peak/background (in sec.) were

20/10 for Si, and 10/5 for other elements in feldspars and micas. Compositional X-ray maps were collected at 15 kV, 100 nA, 100 ms dwell time, 0.33 μm step size and 0.3 μm beam size.
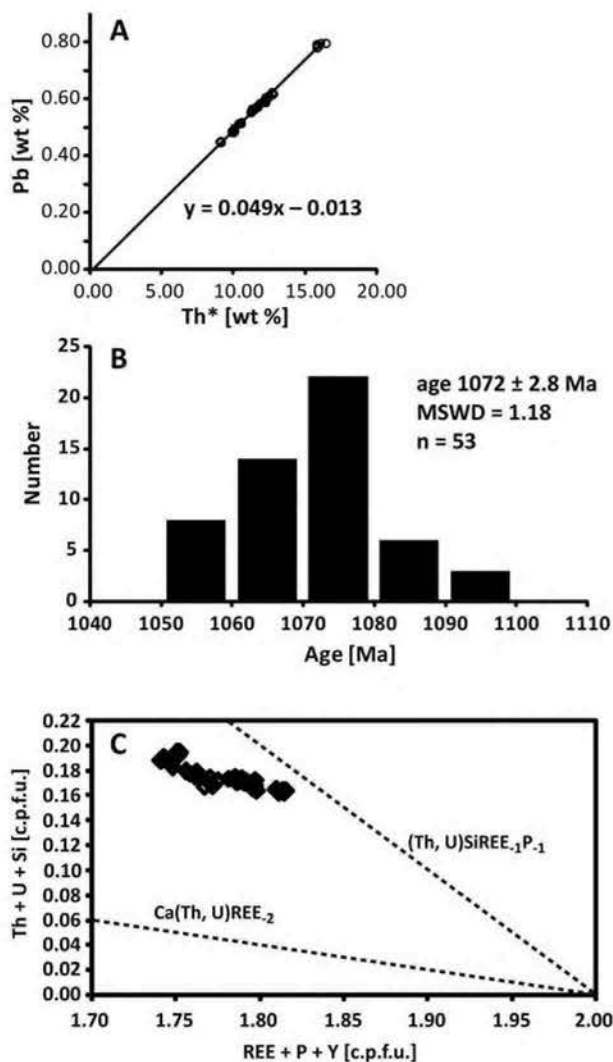
Experiments

The experiments were performed at the Deutsche Geo-ForschungsZentrum (Potsdam, Germany), using cold-seal autoclaves on a hydrothermal line. The P-T conditions used and corresponding duration of the experiments were 250 °C, 200 MPa, 40 days; 350 °C, 200 MPa, 40 days; and 350 °C, 400 MPa, 20 days (Table 1). The experiments utilized an assemblage of monazite + K-feldspar + albite Ab_{100} (or labradorite $An_{60}Ab_{37}Kfs_3$) + muscovite + biotite + synthetic SiO_2 + CaF_2 (Suprapur, Merck). Amorphous SiO_2 was used instead of quartz to increase the reaction rate and CaF_2 was used as a source of Ca and F to form fluorapatite.

The monazite used in the experiments originated from a pegmatite in Burnet County, Texas, U.S.A. A fragment of the monazite crystal was crushed and sieved to obtain the 50–250 μm fraction. Optically clear to foggy, reddish brown grains were hand-picked under the binocular microscope, followed by washing in ethanol in an ultrasonic bath. The grains revealed faint zonation and patchiness in the cross-section under high-contrast backscattered electron (BSE) imaging, which is mostly related to the variation in ThO_2, ranging from 9.40 to 16.95 wt % (Table 2). The Th-U-total Pb age of the monazite was constrained to 1072 ± 2.8 Ma (MSWD = 1.18, n = 53; Fig. 1; Appendix 3) using the electron microprobe. A similar Th-U-total Pb age of 1096 ± 8 Ma was previously obtained by M. J. Jercinovic (in Ruschel et al., 2012).

The selected silicate mineral assemblage is similar to the assemblage used in previous experiments by Budzyń et al. (2011). The minerals included a hydrothermal albite (Ab_{100}; Rožňava, Slovak Republic), labradorite ($An_{60}Ab_{27}Kfs_3$; Chihuahua, Mexico), sanidine (Eifel region, Germany), muscovite from a pegmatite (Siedlimowice, Sudetes, Poland), and biotite (gneiss, Sikkim Himalaya, India). The minerals were crushed and sieved to a 50–250 μm fraction, followed by washing in ethanol in an ultrasonic bath. The foreign or altered mineral grains were hand-picked under a binocular microscope. The fluids used included 2M $Ca(OH)_2$ to test if allanite would form in terms of the relative stabilities of monazite and allanite, and $Na_2Si_2O_5$ + H_2O to test for the remobilization of REE, Th, U and Pb, and to maintain Th-U-total Pb ages of monazite. Solid mixes were prepared by mixing the weighed portions of individual minerals together dry (Table 1). The mineral mix and fluid were loaded into Au capsules, 3 mm wide and 15 mm long, that were arc-welded shut using a Lampert PUK U3 argon plasma torch. The capsules were checked for leaks by first weighing, then placing them in a 105 °C oven overnight, and then weighing them again.

Experiments were conducted using a standard cold-seal, 6 mm bore, René metal autoclaves with H_2O as the pressure medium. Four gently flattened Au capsules, two for monazite (this study) and two for subsequent xenotime experiments (Budzyń and Kozub-Budzyń, 2015), were placed in each of

Fig. 1. The characteristics of the Burnet monazite used in the experiments. A, B. Results of Th-U-total Pb dating of the Burnet monazite. C. Plot of formula proportions of (REE + Y + P) vs. (Th + U + Si), calculated on the basis of 4 oxygen atoms, presenting huttonitic substitution of $(Th, U)SiREE_{-1}P_{-1}$ and cheralitic substitution of $Ca(Th, U)REE_{-2}$ (cf., Förster, 1998; Linthout, 2007).

three autoclaves with Ni-NiO filler rods. Pressures were stable during the experiments. Temperatures were measured externally, with the tip of a Ni-Cr thermocouple, placed in a special hole drilled into the autoclave near the location of the capsules, and are believed to be accurate to within ± 5 °C. After a run, the autoclaves were quenched using compressed air, reaching temperatures of ca. 100 °C within 1 min. The capsules were cleaned, weighed, opened, and dried at 105 °C. Part of the experimental products extracted from a Au capsule was mounted in epoxy and polished. A second part of the reacted mineral mix was sprinkled on the SEM mount with adhesive carbon tape and carbon coated for BSE imaging.

Table 1

Experimental conditions and starting materials (mg)

Exp.	T [°C]	P [MPa]	Duration [days]	Mnz	Ab	Lbr	Kfs	Bt	Ms	SiO₂	CaF₂	Ca(OH)₂	Na₂Si₂O₅	H₂O	Total	Total in Au capsule*	Solids added	Mineral products	Remarks
M12 C-04	250	200	40	5.18	-	3.97	3.03	4.00	2.03	3.92	2.85	0.79	-	5.22	30.99	30.36	25.14	Wo	Starting minerals are not altered. Wollastonite formed.
M12 C-05	350	200	40	5.12	-	4.21	3.08	3.91	1.99	3.87	2.84	0.78	-	5.29	31.09	30.85	25.56	Wo	Starting minerals are not altered. Wollastonite formed.
M12 C-15	350	400	20	5.00	-	4.05	3.40	4.05	2.30	3.97	3.10	0.79	-	5.27	31.93	31.10	25.83	REE-Ap	Delicate crystals of REE-enriched apatite formed on the monazite surface.
M12 N-04	250	200	40	5.28	4.18	-	3.03	4.09	1.88	3.89	3.26	-	5.05	5.15	35.81	35.36	30.21	Stc	Monazite shows strong dissolution with porosity and patchy internal zoning. K-feldspar achived albite rims. Small steacyite grains formed.
M12 N-05	350	200	40	5.12	4.08	-	2.96	3.83	1.73	4.61	2.80	-	4.26	5.56	34.95	33.79	28.23	REE-Ap, Stc, Amph	Monazite shows strong dissolution with porosity along whole grains, and patchy internal zoning. Delicate crystals of REE-rich steacyite and REE-enriched apatite are present on the monazite surface. Large grains of REE-rich steacyite also formed. K-feldspar achieved albite rims. Delicate needle-like crystals of amphiboles are present.
M12 N-15	350	400	20	5.15	4.28	-	3.25	3.98	2.15	4.01	3.02	-	5.09	5.36	36.29	35.43	30.07	REE-Ap, Stc, Amph	Monazite shows strong dissolution with porosity along whole grains, and patchy internal zoning. Numerous, elongated grains of REE-enriched apatite to fluorcalciobritholite formed. REE-rich steacyite formed. K-feldspar achived albite rims. Delicate needle-like crystals of amphiboles are present.

* Difference between Total and Total in Au capsule is related to weight loss during charging the capsule with solids. Ab – albite, Amph – amphibole, Bt – biotite, Kfs – K-feldspar, Lbr – labradorite, Mnz – monazite, Ms – muscovite, REE-Ap – REE-enriched apatite, Stc – REE-rich steacyite, Wo – wollastonite.

EXPERIMENTAL RESULTS

Experiments with 2M Ca(OH)₂

The monazite and other starting minerals showed no signs of alteration (Fig. 2), except for the formation of tiny crystals of REE-enriched apatite on the surface of monazite from the run at 350 °C and 400 MPa (M12C-15). Wollastonite was the second phase formed under conditions of 250–350 °C and 200 MPa (Fig. 2B, C). The chemical composition of monazite, feldspars and micas after the experiments showed no differences with respect to composition of the original minerals (Table 2; Appendix 1 and 2). The small size of the wollastonite and REE-enriched apatite prevented accurate electron microprobe analyses and both phases were identified using SEM-EDS analyses.

Experiments with Na₂Si₂O₅ + H₂O

Alteration of the monazite, including dissolution pits developed on the grain surfaces, was observed in all runs (Fig. 3A, E, H). In cross-section, porosity developed along the monazite rims under conditions of 250 °C and 200 MPa,

leaving the cores unaltered (M12N-04; Fig. 3A). The porosity across whole grains formed at 350 °C and 200 MPa (M12N-05; Fig. 3C, D). The monazite with developed pores showed also patchy zoning under high-contrast BSE imaging (Fig. 3C). Increasing pressure to 400 MPa at the same temperature of 350 °C resulted in the development of porosity in the monazite, filled with a phase showing a composition similar to that of steacyite [(K,□)(Na, Ca)₂(Th, U)Si₈O₂₀], significantly enriched in REE (Table 3). The experimental products included a rare alteration texture of the monazite with pores showing preferred orientation and filled with REE-rich steacyite, across the monazite rim, and a weakly preserved unaltered monazite core (Fig. 4A).

The chemical composition of the monazite differed in both bright and dark compositional domains (Table 2, Figs 3, 4A). The bright areas had a composition, similar to that of the original Burnet monazite. The most noticeable compositional changes in the dark patches were related to a depletion in PbO to 0.01–0.18 wt % *vs.* 0.48–0.86 wt % in the original Burnet monazite. Also UO₂ was depleted to 0.04–0.14 wt % in the dark areas *vs.* 0.26–0.49 wt % in the Burnet monazite. The ThO₂ content in the dark areas varied from

Table 2

Average results of the electron microprobe analyzes of monazite

Sample	T [°C]	P [MPa]	duration [days]	n	P_2O_5	As_2O_5	SiO_2	ThO_2	UO_2	Al_2O_3	Y_2O_3	La_2O_3	Ce_2O_3	Pr_2O_3	Nd_2O_3	Sm_2O_3	Eu_2O_3	Gd_2O_3	Tb_2O_3	Dy_2O_3	Ho_2O_3	Er_2O_3	Tm_2O_3	Yb_2O_3	Lu_2O_3	CaO	FeO	SrO	PbO	SO_3	Total
Burnet Monazite				53	27.00	0.13	1.74	11.82	0.35	<0.02	0.92	8.48	27.34	3.47	9.34	3.96	<0.08	1.83	0.33	1.27	<0.09	0.45	0.11	0.19	0.13	1.23	0.11	<0.03	0.60	<0.02	100.79
					0.40	*0.01*	*0.10*	*2.03*	*0.06*		*0.32*	*0.94*	*2.81*	*0.26*	*0.53*	*0.68*		*0.48*	*0.11*	*0.42*		*0.05*	*0.01*	*0.03*	*0.02*	*0.49*	*0.06*		*0.11*		
M12C-04	250	200	40	20	26.54	0.13	1.81	11.44	0.33	<0.02	0.85	8.38	27.57	3.50	9.26	3.88	<0.08	1.80	0.30	1.18	<0.09	0.43	0.09	0.18	<0.09	1.10	<0.02	<0.03	0.59	0.02	99.39
unaltered					*0.50*	*0.01*	*0.08*	*0.79*	*0.01*		*0.13*	*0.43*	*1.16*	*0.11*	*0.21*	*0.34*		*0.20*	*0.04*	*0.18*		*0.03*	*0.02*	*0.02*		*0.17*	*0.06*		*0.04*	*0.01*	
M12C-05	350	200	40	19	26.99	0.14	1.72	11.19	0.33	<0.02	0.87	8.61	27.64	3.50	9.32	3.87	<0.08	1.78	0.32	1.17	<0.09	0.43	<0.09	0.17	0.12	1.12	<0.02	<0.03	0.58	<0.02	99.84
unaltered					*0.44*	*0.00*	*0.15*	*1.21*	*0.04*		*0.27*	*0.96*	*2.37*	*0.17*	*0.24*	*0.74*		*0.46*	*0.10*	*0.38*		*0.05*	*0.03*	*0.03*	*0.01*	*0.36*			*0.06*		
M12C-15	350	400	20	20	27.06	0.05	1.70	11.54	0.34	<0.02	0.89	8.31	27.02	3.44	9.20	3.90	<0.08	1.84	0.32	1.22	<0.09	0.45	0.10	0.18	0.13	1.12	<0.02	<0.03	0.59	0.02	99.41
unaltered					*0.56*	*0.05*	*0.13*	*1.05*	*0.05*		*0.21*	*0.62*	*1.79*	*0.15*	*0.35*	*0.49*		*0.32*	*0.08*	*0.28*		*0.04*	*0.02*	*0.03*	*0.03*	*0.30*			*0.05*	*0.00*	
M12N-04	250	200	40	9	26.55	0.08	1.70	12.51	0.36	<0.02	1.04	7.82	25.73	3.31	9.00	4.24	<0.08	2.11	0.37	1.42	<0.09	0.45	0.10	0.20	<0.09	1.41	<0.02	<0.03	0.63	0.02	99.06
unaltered					*0.45*	*0.06*	*0.14*	*0.28*	*0.02*		*0.14*	*0.22*	*0.87*	*0.09*	*0.11*	*0.22*		*0.23*	*0.05*	*0.14*		*0.03*	*0.02*	*0.02*		*0.16*			*0.01*	*0.00*	
M12N-04				10	27.25	0.09	1.28	5.04	0.09	<0.02	0.26	10.43	32.80	4.00	10.45	3.52	<0.08	1.16	0.14	0.41	<0.09	0.32	0.09	0.14	<0.09	0.85	<0.02	0.08	0.14	0.03	98.55
altered					*0.39*	*0.06*	*0.11*	*0.75*	*0.03*		*0.09*	*0.37*	*1.10*	*0.07*	*0.29*	*0.23*		*0.22*	*0.03*	*0.10*		*0.02*	*0.01*	*0.02*		*0.09*		*0.02*	*0.04*	*0.00*	
M12N-05	350	200	40	7	26.57	0.13	1.81	13.46	0.38	<0.02	1.18	7.59	24.79	3.26	8.77	4.27	<0.08	2.14	0.39	1.49	<0.09	0.47	0.11	0.22	0.10	1.52	<0.02	<0.03	0.68	0.02	99.35
unaltered					*0.47*	*0.00*	*0.13*	*1.03*	*0.04*		*0.33*	*0.64*	*2.36*	*0.25*	*0.46*	*0.43*		*0.42*	*0.09*	*0.36*		*0.04*	*0.01*	*0.02*	*0.01*	*0.37*			*0.05*	*0.01*	
M12N-05				11	26.25	0.13	1.88	5.65	0.06	<0.02	0.17	10.79	33.31	3.99	10.23	3.48	<0.08	1.24	0.15	0.42	<0.09	0.30	0.09	0.14	0.10	0.34	<0.02	<0.03	0.06	0.02	98.80
altered					*0.86*	*0.01*	*0.33*	*2.95*	*0.04*		*0.15*	*1.13*	*2.16*	*0.17*	*0.21*	*0.28*		*0.27*	*0.07*	*0.30*		*0.05*	*0.02*	*0.03*	*0.01*	*0.21*			*0.06*	*0.00*	
M12N-15	350	400	20	9	26.78	0.14	1.66	9.94	0.29	<0.02	0.76	9.68	28.79	3.54	9.91	2.87	<0.08	1.38	0.19	0.72	<0.09	0.39	0.11	0.16	0.11	0.83	<0.02	<0.03	0.51	0.02	98.78
unaltered					*0.30*	*0.01*	*0.28*	*0.12*	*0.01*		*0.40*	*0.77*	*1.85*	*0.26*	*0.58*	*0.31*		*0.16*	*0.04*	*0.12*		*0.04*	*0.02*	*0.03*	*0.01*	*0.28*			*0.01*	*0.01*	
M12N-15				10	27.04	0.14	1.82	3.73	0.05	<0.02	0.11	11.51	34.12	4.06	10.51	3.02	<0.08	1.09	0.11	0.24	<0.09	0.29	0.08	0.13	<0.09	0.33	<0.02	<0.03	0.06	0.03	98.48
altered					*0.77*	*0.00*	*0.65*	*1.15*	*0.02*		*0.04*	*0.78*	*0.93*	*0.15*	*0.40*	*0.47*		*0.15*	*0.04*	*0.06*		*0.02*	*0.01*	*0.02*		*0.07*			*0.05*	*0.01*	

Comments: all values are given in wt %; Italic - standard deviation
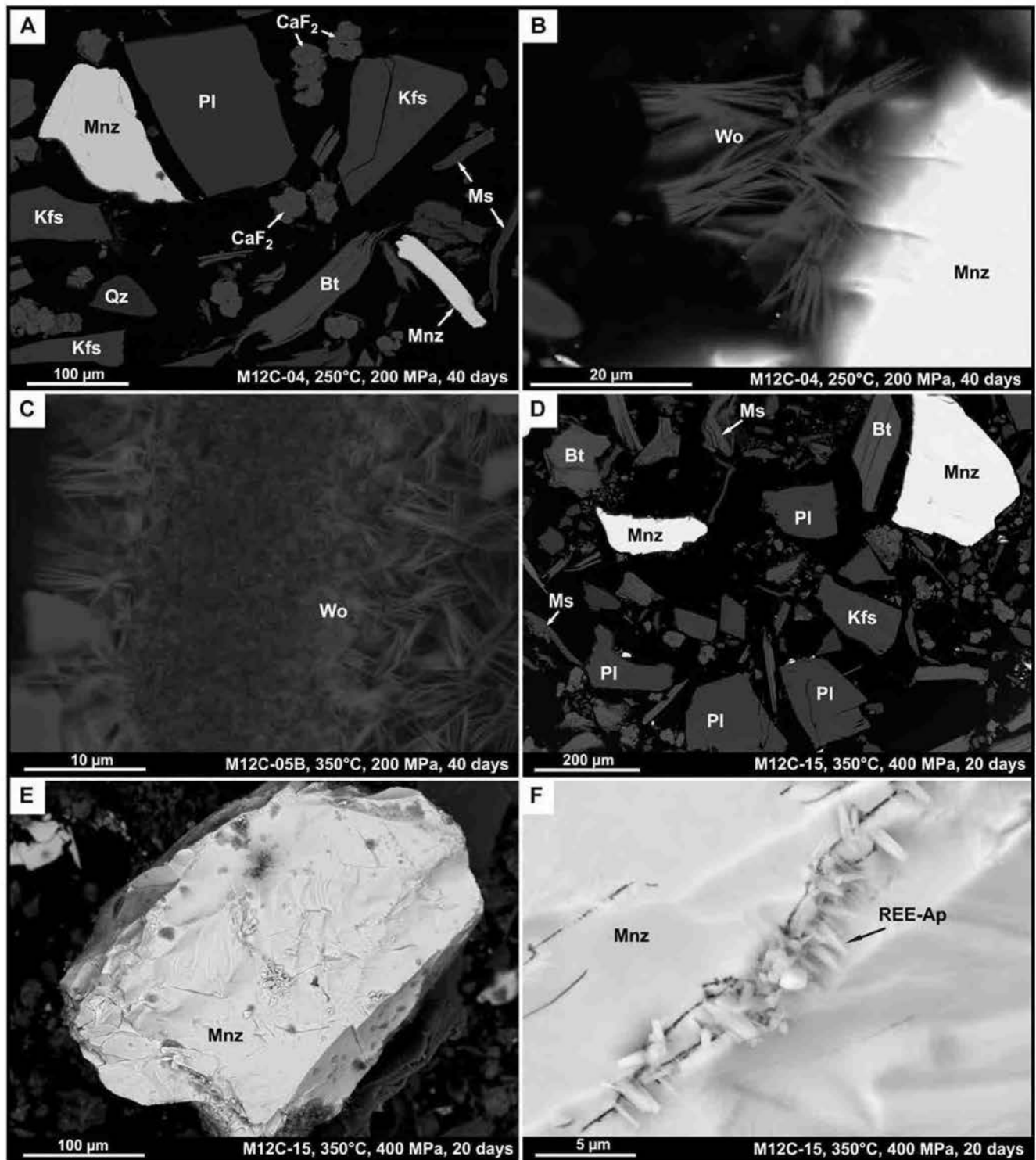
Fig. 2. Experimental products from runs with 2M $Ca(OH)_2$ fluid. A. Mineral phases after experiment at 250 °C, 200 MPa, 40 days, showing no alteration with respect to starting minerals. B, C. Wollastonite formed in runs at 250 °C, 200 MPa, 40 days (B), and 350 °C, 200 MPa, 40 days (C). D, E. Minerals showing no alterations after run at 350 °C, 400 MPa, 20 days. F. REE-enriched apatite formed in run at 350 °C, 400 MPa, 20 days. Mineral abbreviations: Bt – biotite, Kfs – K-feldspar, Mnz – monazite, Ms – muscovite, Qz – quartz, Pl – plagioclase, REE-Ap – REE-enriched apatite, Wo – wollastonite.

3.53 to 9.75 wt %, while the Burnet monazite contained 9.40–16.95 wt % ThO_2. Actinide depletion was accompanied by an increased LREE concentration of 56.90–64.02 wt % $(LREE_{-Gd})_2O_3$ *vs.* 43.95–58.17 wt % in the Burnet monazite. In contrast, Y, Gd and HREE were depleted in the

dark patches, 1.63–3.74 wt % $(Y, Gd, HREE)_2O_3$ *vs.* 2.82–7.86 wt % in the Burnet monazite. The specific dependence on P-T reflected substitution of Si. The dark areas contained 1.15–1.43 wt % SiO_2 in the monazite from the 250 °C and 200 MPa run, and 1.87–3.46 wt % SiO_2 in the monazite
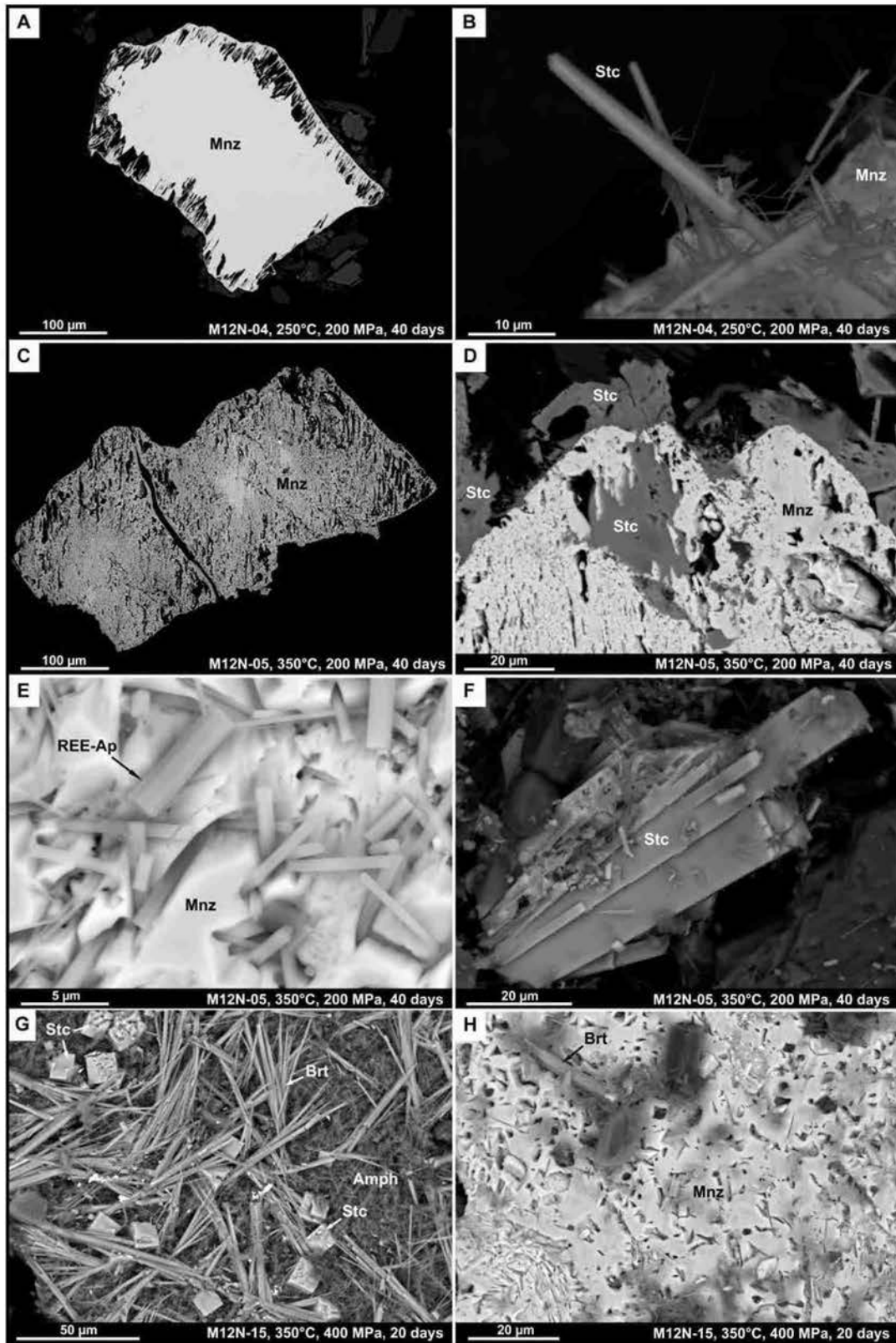
Fig. 3. Experimental products from runs with $Na_2Si_2O_5 + H_2O$ fluid. A. Altered monazite with developed porosity along rim in run at 250 °C, 200 MPa and 40 days. B. REE-rich steacyite crystals formed on the monazite surface. C. Altered monazite with developed patchy zoning and porosity in run at 350 °C, 200 MPa and 40 days. D. Intergrowth of altered monazite with REE-rich steacyite formed at 350 °C, 200 MPa and 40 days. E. Crystals of REE-enriched apatite on the monazite surface from 350 °C, 200 MPa and 40 days run. F. Pristine, euhedral crystals of REE-rich steacyite from 350 °C, 200 MPa and 40 days run. G. Crystals of REE-rich steacyite, fluorcalciobritholite and amphibole on the surface of monazite (350 °C, 400 MPa and 20 days run). H. Partially dissolved surface of the monazite with second-ary fluorcalciobritholite crystal from 350 °C, 400 MPa and 20 days run. Mineral abbreviations: Amph – amphibole, Brt – fluorcalcio-britholite, Mnz – monazite, REE-Ap – REE-enriched apatite, Stc – REE-rich steacyite.
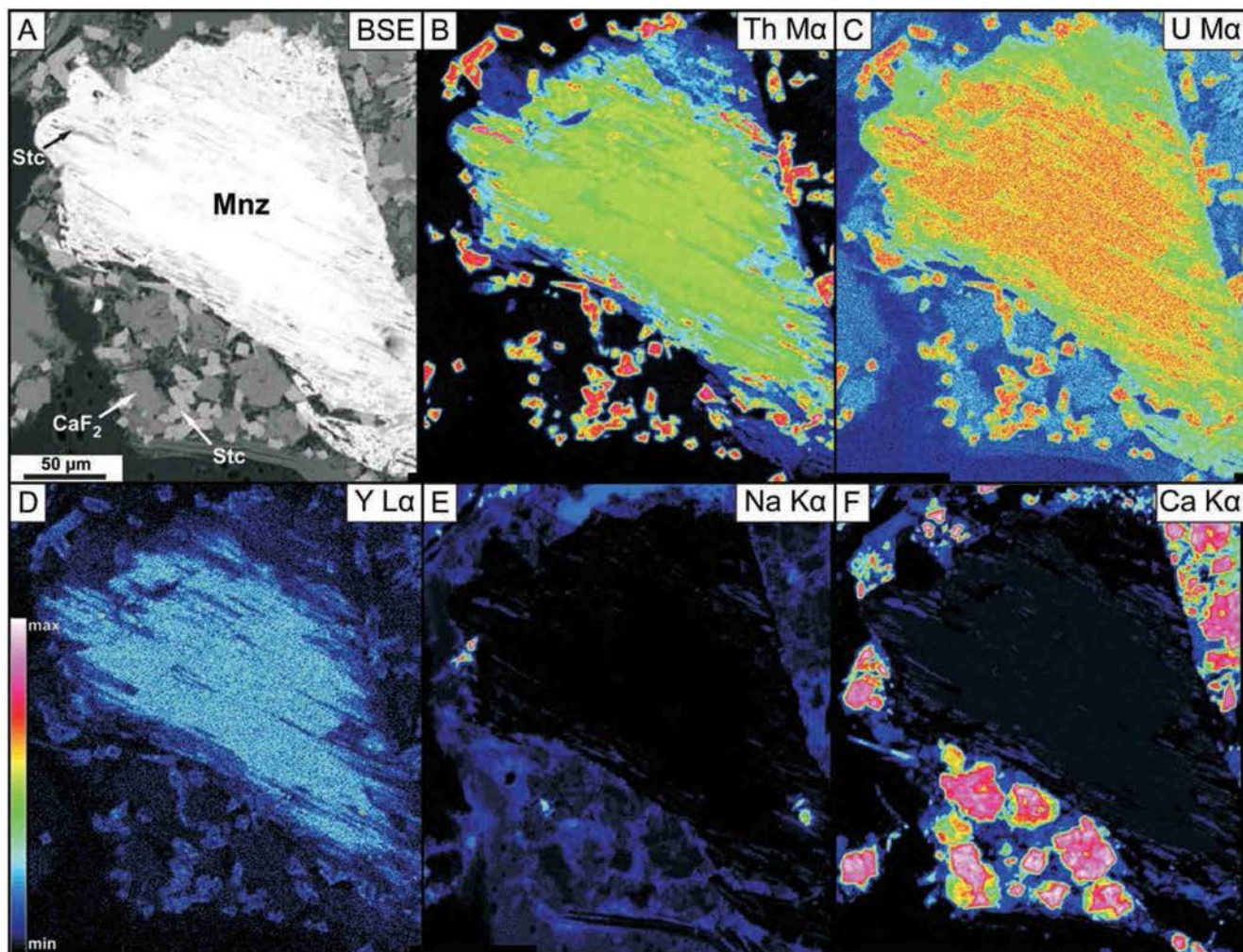
Fig. 4.   BSE image (A) and X-ray compositional maps (B–F) of monazite altered under experimental conditions of 350 °C, 400 MPa, 20 days. All images are in the same scale. The colour scale representing increasing element concentration in the lower left corner is common for all X-ray maps; however, please note that the intensities are not necessarily correlated.

from the 350 °C and 200–400 MPa runs, *vs.* 1.52–1.90 wt % SiO_2 in the Burnet monazite. Depletion of Ca in the dark patches of the monazite increased with increasing P-T conditions, from 0.72–0.85 wt % CaO in the 250 °C and 200 MPa run; 0.26–0.73 wt % CaO in the 350 °C and 200 MPa run; to 0.29–0.37 wt % CaO in the 350 °C and 400 MPa run, *vs.* 0.57–2.38 wt % CaO in the Burnet monazite. The compositional diagrams of REE + P + Y *vs.* Th + U + Si (Fig. 5) show that the huttonite substitution dominated in the dark compositional domains, interpreted as altered domains, while both the huttonite and cheralite substitutions occurred in the Burnet monazite and bright unaltered areas in the monazite from the experimental products.

The REE-enriched apatite- to fluorcalciobritholite formed only in the runs at 350 °C and 200–400 MPa (Fig. 3E, G, H). The concentration of $(Y + REE)_2O_3$ in the REE-enriched apatite- to fluorcalciobritholite ranges from 33.87 to 37.57 wt %, and 29.59 to 31.10 wt % in the M12N-05 and M12N-15 runs, respectively (Table 4).

The REE-rich steacyite crystallized in all experiments. It formed <20 μm, prismatic crystals on the monazite surface in the run at 250 °C and 200 MPa (Fig. 3B). Under

higher temperatures of 350 °C (both 200 and 400 MPa runs), REE-rich steacyite formed anhedral grains replacing monazite (Fig. 3D) or euhedral tetragonal crystals reaching up to 80 μm in size (Fig. 3F, G). Also, in both runs at 350 °C, REE-rich steacyite filled the pores showing preferred orientation in monazite grains (Fig. 4A). The chemical composition of the REE-rich steacyite varied depending on P-T conditions. The ThO_2 content decreased with increasing P-T conditions from 22.15 to 24.46 wt % (250 °C and 200 MPa), 18.49 to 22.34 wt % (350 °C and 200 MPa) to 17.70 to 18.15 wt % (350 °C and 400 MPa). Subsequently, an increase of P-T conditions promoted the incorporation of REE from 4.54 to 5.21 wt % $(Y, REE)_2O_3$ (250 °C and 200 MPa), 5.09 to 8.04 wt % (350 °C and 200 MPa) to 8.17 to 9.02 wt % (350 °C and 400 MPa). There was no specific pattern in U content. A second trend from runs at 250 °C and 200 MPa to 350 °C, 400 MPa were observed in decreasing Na_2O concentrations from 4.11 wt % to 2.71 wt %, and CaO increasing from 6.19 to 9.00 wt %, respectively.

Albite showed no alteration (Appendix 1). K-feldspar was rimmed by secondary albite (Appendix 1). Muscovite and biotite retained the composition of the starting micas

Table 3

Results of the electron microprobe analyzes of REE-rich steacyite formed in experiments with $Na_2Si_2O_5 + H_2O$ fluid

Analysis	Comment	P_2O_5	SiO_2	TiO_2	ThO_2	UO_2	Al_2O_3	Y_2O_3	La_2O_3	Ce_2O_3	Pr_2O_3	Nd_2O_3	Sm_2O_3	Eu_2O_3	Gd_2O_3	Tb_2O_3	Dy_2O_3	Ho_2O_3	Er_2O_3	Tm_2O_3	Yb_2O_3	Lu_2O_3	MgO	CaO	MnO	FeO	SrO	PbO	Na_2O	K_2O	F	Cl	Total	$(Y+REE)_2O_3$
														M12N-04, 250°C, 200 MPa, 40 days																				
1-1	Mnz-int	<0.02	56.63	0.12	24.46	0.42	<0.02	0.55	<0.08	0.67	0.31	0.63	0.71	0.13	0.76	0.21	0.58	n.a.	n.a.	n.a.	n.a.	n.a.	<0.01	6.19	<0.01	0.09	<0.01	<0.05	4.11	4.39	<0.01	<0.01	100.95	4.54
2-1	Mnz-int	<0.02	57.61	<0.02	22.15	0.56	<0.02	0.81	<0.08	0.44	0.13	0.49	0.90	0.15	1.05	0.22	1.03	n.a.	n.a.	n.a.	n.a.	n.a.	<0.01	6.19	<0.01	0.06	0.04	<0.05	4.18	5.04	<0.01	<0.01	101.04	5.21
														M12N-05, 350°C, 200 MPa, 40 days																				
1-1	matrix	<0.02	56.96	0.22	22.34	0.79	<0.02	0.71	<0.08	0.75	0.29	0.64	0.71	0.12	0.85	0.22	0.79	n.a.	n.a.	n.a.	n.a.	n.a.	<0.01	7.02	<0.01	0.09	0.06	<0.05	4.75	3.13	<0.01	<0.01	100.45	5.09
1-2	matrix	0.03	57.18	0.07	20.86	0.66	0.03	0.85	<0.08	0.89	0.38	0.81	0.96	0.10	1.06	0.26	1.14	n.a.	n.a.	n.a.	n.a.	n.a.	<0.01	7.99	<0.01	0.09	0.03	<0.05	4.35	3.21	<0.01	<0.01	100.95	6.45
2-1	Mnz-int	1.20	55.31	0.09	19.70	0.81	<0.02	1.21	0.13	0.82	0.31	0.70	0.78	<0.09	1.06	0.28	1.31	n.a.	n.a.	n.a.	n.a.	n.a.	0.09	7.80	0.02	0.44	<0.01	0.06	3.86	4.57	<0.01	<0.01	100.55	6.60
3-1	Mnz-int	<0.02	57.78	<0.02	18.58	0.44	<0.02	1.67	<0.08	0.63	0.27	0.63	1.04	<0.09	1.43	0.41	1.96	n.a.	n.a.	n.a.	n.a.	n.a.	<0.01	7.87	<0.01	<0.01	<0.01	<0.05	3.49	4.71	<0.01	<0.01	100.92	8.04
3-2	Mnz-int	<0.02	57.40	<0.02	18.49	0.41	<0.02	1.79	<0.08	0.54	0.24	0.62	0.98	<0.09	1.44	0.41	1.95	n.a.	n.a.	n.a.	n.a.	n.a.	<0.01	7.86	0.03	0.02	<0.01	<0.05	3.24	4.73	<0.01	<0.01	100.16	7.97
														M12N-15, 350°C, 400 MPa, 20 days																				
1-1	matrix	<0.02	57.42	0.05	17.88	0.50	<0.01	0.83	<0.08	1.21	0.39	1.30	1.64	<0.09	1.51	0.36	1.23	<0.10	0.36	<0.08	0.18	<0.14	<0.01	8.26	<0.01	0.10	0.03	<0.05	2.71	5.22	<0.01	<0.01	101.19	9.02
1-2	matrix	<0.02	57.17	0.06	17.70	0.54	<0.01	0.57	0.20	1.72	0.44	1.59	1.59	<0.09	1.33	0.25	1.01	<0.10	0.28	<0.08	0.16	0.18	<0.01	9.00	0.02	0.03	<0.01	<0.05	2.72	4.94	<0.01	<0.01	101.50	9.32
2	matrix	<0.02	56.60	0.05	17.74	0.50	<0.01	0.44	0.18	1.59	0.45	1.48	1.54	<0.09	1.38	0.24	0.89	<0.10	0.23	<0.08	0.00	<0.14	<0.01	8.93	<0.01	<0.01	<0.01	<0.05	2.82	4.48	<0.01	<0.01	99.55	8.42
3	matrix	<0.02	56.62	<0.02	18.15	0.61	<0.01	1.28	<0.08	0.88	0.37	0.87	1.12	<0.09	1.22	0.32	1.43	<0.10	0.46	<0.08	0.23	<0.14	<0.01	7.84	<0.01	0.04	<0.01	<0.05	2.85	5.17	<0.01	<0.01	99.45	8.17
4	matrix	<0.02	57.18	0.06	17.94	0.54	<0.01	0.39	0.15	1.77	0.47	1.53	1.46	<0.09	1.20	0.27	0.79	<0.10	0.29	<0.08	0.10	<0.14	<0.01	8.94	<0.01	<0.01	0.03	<0.05	2.85	4.55	<0.01	<0.01	100.53	8.41

[c.p.f.u.]

Analysis	Comment	P	Si	Ti	Th	U	Al	Y	La	Ce	Pr	Nd	Sm	Eu	Gd	Tb	Dy	Ho	Er	Tm	Yb	Lu	Mg	Ca	Mn	Fe	Sr	Pb	Na	K	F	Cl	Total	Y+REE
														M12N-04, 250°C, 200 MPa, 40 days																				
1-1	Mnz-int	0.000	7.935	0.013	0.780	0.013	0.000	0.041	0.000	0.034	0.016	0.031	0.034	0.006	0.035	0.010	0.026	n.a.	n.a.	n.a.	n.a.	n.a.	0.000	0.929	0.000	0.011	0.000	0.000	1.116	1.340	0.000	0.000	12.370	0.234
2-1	Mnz-int	0.000	7.961	0.004	0.696	0.017	0.000	0.059	0.000	0.022	0.006	0.024	0.043	0.007	0.048	0.010	0.046	n.a.	n.a.	n.a.	n.a.	n.a.	0.000	0.916	0.000	0.007	0.003	0.000	1.119	1.519	0.000	0.000	12.509	0.266
														M12N-05, 350°C, 200 MPa, 40 days																				
1-1	matrix	0.000	7.953	0.023	8.710	0.025	0.000	0.052	0.000	0.039	0.015	0.032	0.034	0.005	0.039	0.010	0.036	n.a.	n.a.	n.a.	n.a.	n.a.	0.000	1.050	0.000	0.011	0.005	0.000	1.287	0.953	0.000	0.000	12.278	0.263
1-2	matrix	0.003	7.925	0.008	0.658	0.020	0.005	0.063	0.000	0.045	0.019	0.040	0.046	0.004	0.049	0.012	0.051	n.a.	n.a.	n.a.	n.a.	n.a.	0.000	1.187	0.000	0.010	0.003	0.000	1.168	0.970	0.000	0.000	12.286	0.329
2-1	Mnz-int	0.141	7.681	0.009	0.623	0.025	0.000	0.090	0.007	0.042	0.016	0.035	0.037	0.004	0.049	0.013	0.059	n.a.	n.a.	n.a.	n.a.	n.a.	0.019	1.160	0.003	0.052	0.000	0.002	1.038	1.384	0.000	0.000	12.487	0.350
3-1	Mnz-int	0.000	7.927	0.000	0.580	0.013	0.000	0.122	0.000	0.032	0.013	0.031	0.049	0.004	0.065	0.018	0.087	n.a.	n.a.	n.a.	n.a.	n.a.	0.000	1.157	0.000	0.000	0.000	0.001	0.929	1.408	0.000	0.000	12.438	0.421
3-2	Mnz-int	0.000	7.929	0.000	0.581	0.013	0.000	0.131	0.000	0.028	0.012	0.030	0.047	0.003	0.066	0.018	0.087	n.a.	n.a.	n.a.	n.a.	n.a.	0.000	1.164	0.004	0.003	0.000	0.002	0.868	1.426	0.000	0.000	12.413	0.423
														M12N-15, 350°C, 400 MPa, 20 days																				
1-1	matrix	0.000	7.896	0.005	0.560	0.015	0.000	0.061	0.000	0.061	0.020	0.064	0.078	0.004	0.069	0.016	0.054	0.000	0.016	0.000	0.008	0.000	0.000	1.216	0.000	0.012	0.002	0.000	0.722	1.566	0.000	0.000	12.444	0.450
1-2	matrix	0.000	7.860	0.006	0.554	0.017	0.000	0.041	0.010	0.087	0.022	0.078	0.075	0.004	0.061	0.011	0.045	0.000	0.012	0.000	0.007	0.008	0.000	1.325	0.003	0.003	0.000	0.000	0.725	1.481	0.000	0.000	12.436	0.461
2	matrix	0.000	7.900	0.006	0.564	0.016	0.000	0.032	0.009	0.081	0.023	0.074	0.074	0.003	0.064	0.011	0.040	0.000	0.010	0.000	0.000	0.000	0.000	1.335	0.000	0.000	0.000	0.000	0.763	1.362	0.000	0.000	12.367	0.422
3	matrix	0.000	7.907	0.000	0.577	0.019	0.000	0.095	0.000	0.045	0.019	0.043	0.054	0.004	0.056	0.015	0.064	0.000	0.020	0.000	0.010	0.004	0.000	1.173	0.000	0.004	0.000	0.000	0.773	1.574	0.000	0.000	12.456	0.429
4	matrix	0.003	7.898	0.006	0.564	0.017	0.000	0.028	0.008	0.090	0.023	0.075	0.069	0.003	0.055	0.012	0.035	0.000	0.013	0.000	0.004	0.004	0.000	1.323	0.000	0.000	0.002	0.000	0.764	1.371	0.000	0.000	12.368	0.420

Notes: cations per formula unit (c.p.f.u.) are calculated on the basis of 20 oxygen atoms; n.a. – not analyzed; matrix – individual grain of REE-steacyite; Mnz-int – REE-rich steacyite intergrown with monazite.

[wt %]	P_2O_5	SiO_2	TiO_2	ThO_2	UO_2	Al_2O_3	Y_2O_3	La_2O_3	Ce_2O_3	Pr_2O_3	Nd_2O_3	Sm_2O_3	Eu_2O_3	Gd_2O_3	Tb_2O_3	Dy_2O_3	Ho_2O_3	Er_2O_3	Tm_2O_3	Yb_2O_3	Lu_2O_3	MgO	CaO	MnO	FeO	SrO	PbO	Na_2O	K_2O	F	Cl	Sum	O=(F+Cl)	total	$(Y+REE)_2O_3$
												M12N-05, 350°C, 200 MPa, 40 days																							
1	26.85	5.80	0.46	2.11	<0.01	0.10	0.45	4.80	15.31	2.41	6.72	3.52	<0.04	2.07	0.28	0.84	n.a.	n.a.	n.a.	n.a.	n.a.	0.35	19.08	0.06	1.72	0.11	0.07	4.67	0.10	3.41	<0.01	101.30	1.44	99.87	36.40
2	29.56	1.76	0.06	2.25	0.04	<0.01	0.57	4.76	15.29	2.40	6.98	3.87	<0.04	2.31	0.32	1.07	n.a.	n.a.	n.a.	n.a.	n.a.	<0.01	23.62	<0.01	0.32	0.14	0.06	3.68	0.04	2.67	0.03	101.78	1.13	100.65	37.57
3	29.70	1.21	<0.01	0.17	<0.01	0.04	0.68	2.92	12.11	2.13	7.15	4.44	<0.04	2.71	0.38	1.35	n.a.	n.a.	n.a.	n.a.	n.a.	<0.01	26.73	0.04	0.05	0.10	0.15	3.89	0.01	1.94	<0.01	97.90	0.81	97.08	33.87
												M12N-15, 350°C, 400 MPa, 20 days																							
1	32.75	0.65	<0.01	0.14	0.22	0.02	0.85	2.65	10.52	1.70	5.87	3.27	0.05	2.18	0.47	1.37	0.05	0.31	0.08	0.09	0.12	<0.01	28.41	<0.01	<0.01	0.26	0.02	3.67	0.09	2.19	<0.01	98.01	0.92	97.09	29.59
2	32.33	0.74	0.03	0.16	0.19	<0.01	0.81	2.50	10.94	1.81	6.45	3.73	<0.04	2.40	0.44	1.55	0.06	0.27	0.06	0.09	<0.04	<0.01	27.63	<0.01	<0.01	0.47	0.02	4.13	0.25	2.19	<0.01	99.25	0.92	98.33	31.10

[c.p.f.u.]	P	Si	Ti	Th	U	Al	Y	La	Ce	Pr	Nd	Sm	Eu	Gd	Tb	Dy	Ho	Er	Tm	Yb	Lu	Mg	Ca	Mn	Fe	Sr	Pb	Na	K	F	Cl	Total	Y+REE
											M12N-05, 350°C, 200 MPa, 40 days																							
1	2.309	0.589	0.035	0.049	0.000	0.012	0.024	0.180	0.569	0.089	0.244	0.123	0.000	0.070	0.009	0.027	0.000	0.000	0.000	0.000	0.000	0.053	2.076	0.007	0.146	0.007	0.002	0.920	0.023	1.096	0.000	8.660	1.336
2	2.595	0.183	0.005	0.053	0.001	0.000	0.032	0.182	0.581	0.091	0.258	0.138	0.000	0.079	0.011	0.036	0.000	0.000	0.000	0.000	0.000	0.000	2.624	0.000	0.028	0.008	0.002	0.739	0.010	0.877	0.005	8.536	1.408
3	2.670	0.129	0.000	0.004	0.000	0.005	0.038	0.114	0.471	0.083	0.271	0.162	0.000	0.095	0.013	0.046	0.000	0.000	0.000	0.000	0.000	0.000	3.041	0.004	0.005	0.006	0.004	0.800	0.002	0.650	0.000	8.614	1.294
											M12N-15, 350°C, 400 MPa, 20 days																							
1	2.816	0.066	0.000	0.003	0.005	0.002	0.046	0.099	0.391	0.063	0.213	0.114	0.002	0.073	0.016	0.045	0.002	0.010	0.003	0.003	0.004	0.000	3.092	0.000	0.000	0.015	0.001	0.723	0.021	0.704	0.000	8.531	1.083
2	2.780	0.075	0.002	0.004	0.004	0.000	0.044	0.094	0.407	0.067	0.234	0.130	0.000	0.081	0.015	0.051	0.002	0.009	0.002	0.003	0.000	0.000	3.007	0.000	0.000	0.028	0.001	0.814	0.056	0.704	0.000	8.611	1.137

Notes: cations per formula unit (c.p.f.u.) are calculated on the basis of 13 oxygen atoms; n.a. – not analyzed.
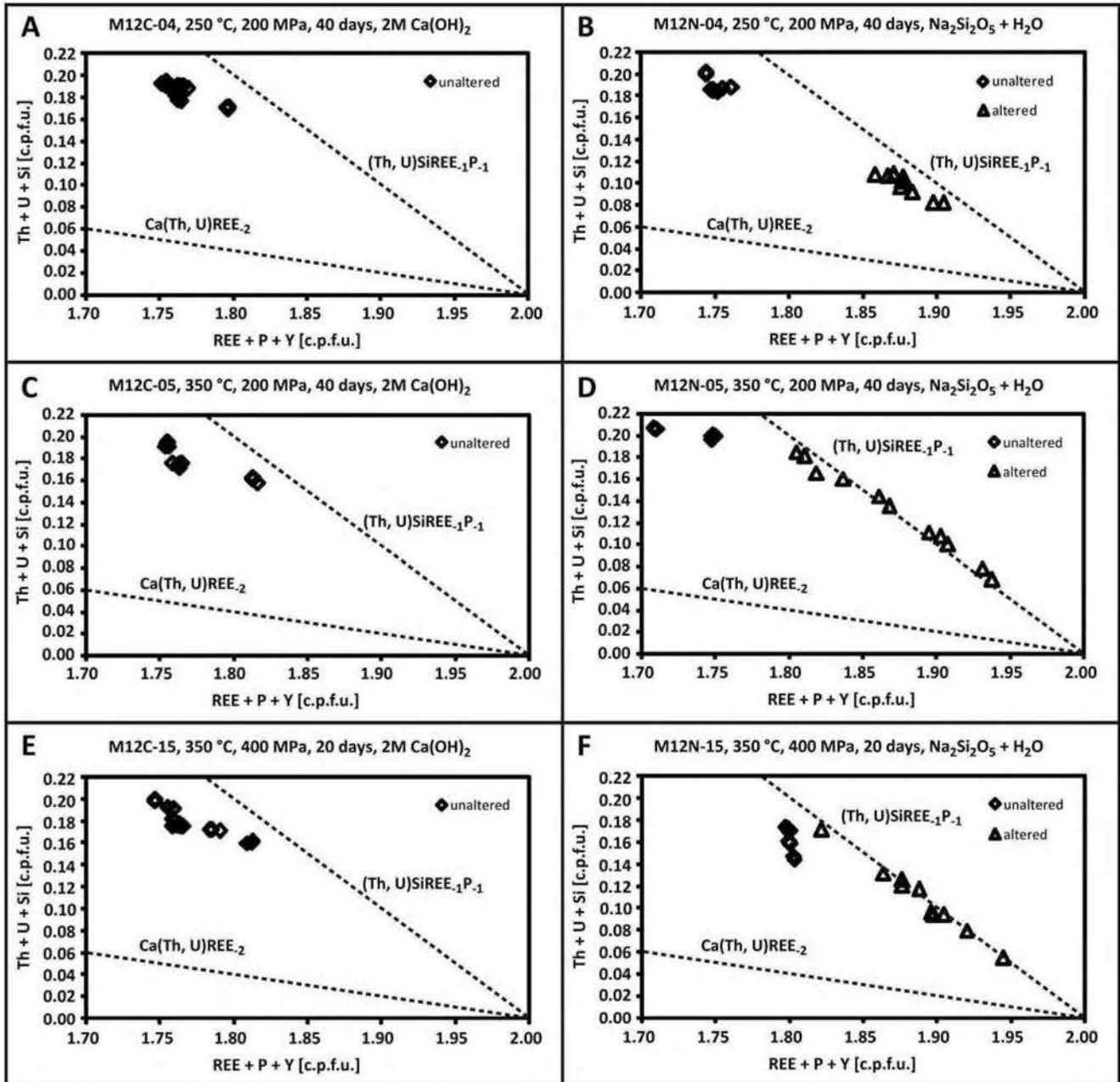
Fig. 5. Plots of formula proportions of (REE + Y + P) vs. (Th + U + Si) calculated on the basis of 4 oxygen atoms for the monazite in experimental products from runs at 250 °C, 200 MPa, 40 days (A, B), 350 °C, 200 MPa, 40 days (C, D) and 350 °C, 400 MPa, 20 days (E, F). The huttonitic substitution of $(Th, U)SiREE_{-1}P_{-1}$ and cheralitic substitution of $Ca(Th, U)REE_{-2}$ are represented by dashed lines (cf., Förster, 1998; Linthout, 2007). The monazite in experimental products from runs with 2M $Ca(OH)_2$ shows pattern similar to that of the starting Burnet monazite. Compositional alteration of the monazite in the presence of $Na_2Si_2O_5$ + H_2O fluid resulted in domination of the huttonitic substitution in the altered domains, whereas the unaltered domains exhibit composition similar to that of the Burnet monazite (Fig. 1C).

(Appendix 2). Delicate needle-like grains of Na- and Fe-rich amphibole formed only in the runs at 350 °C and 200–400 MPa (Fig. 3G).

Maintaining original Th-U-total Pb ages of monazite during experiments

The monazite in the experimental products was analyzed in terms of preserving the original Th-U-total Pb ages.

The monazite from runs with 2M $Ca(OH)_2$ yielded ages of 1095 ± 4.6 Ma (250 °C and 200 MPa), 1100 ± 4.8 Ma (350 °C and 200 MPa), and 1088 ± 5.0 Ma (350 °C, 400 MPa; Fig. 6, Appendix 3). Although slightly shifted, these ages are similar to the 1072 ± 2.8 Ma age of the original Burnet monazite, showing that the Th-U-Pb system in the monazite was not disturbed in experiments with 2M $Ca(OH)_2$.

The patchy zoned monazite from the runs with $Na_2Si_2O_5$ + H_2O yielded various ages. Bright zones under BSE imaging give ages of 1074 ± 6.7 Ma (250 °C and 200 MPa), 1081
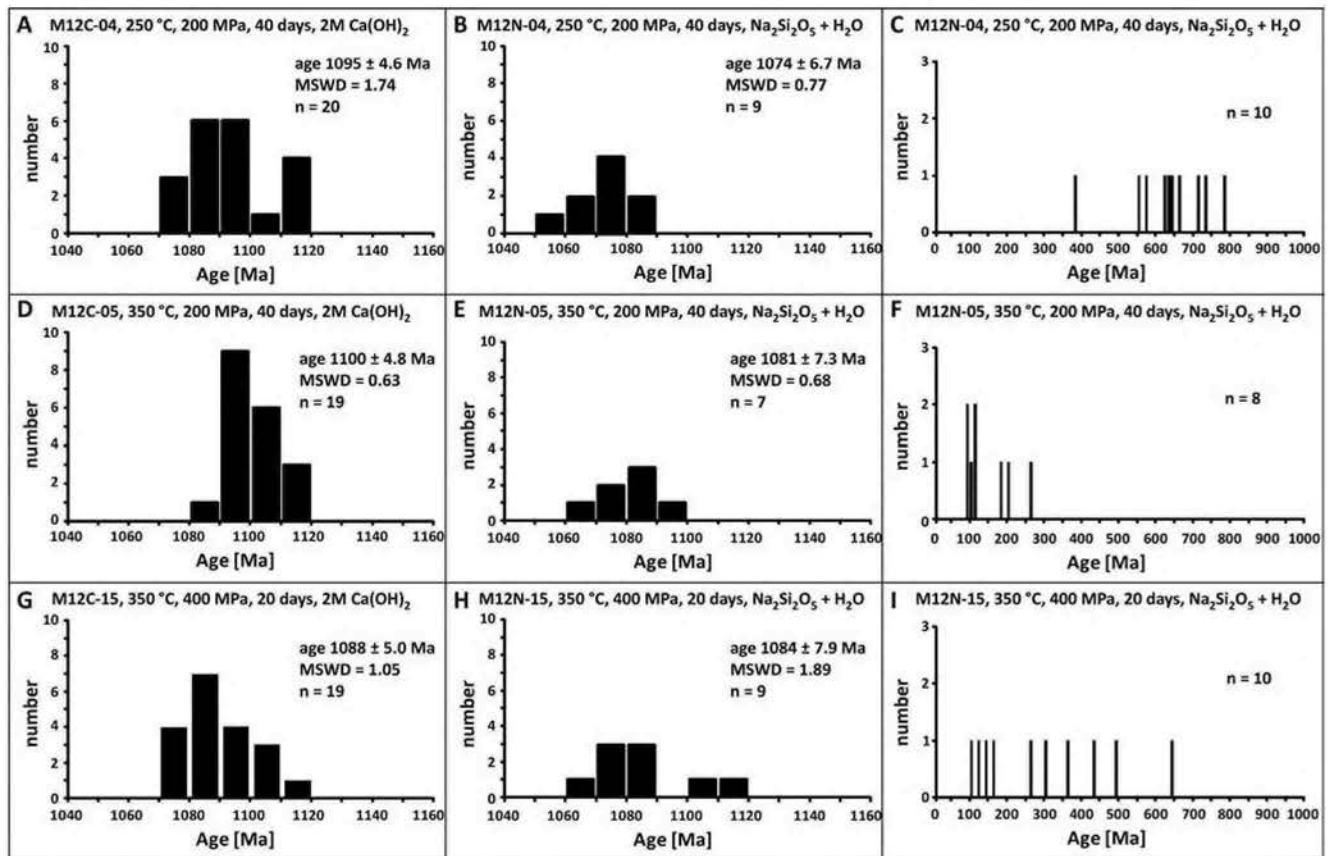
Fig. 6. Results of Th-U-total Pb "dating" of the monazite in experimental products from runs at 250 °C, 200 MPa, 40 days (A–C), 350 °C, 200 MPa, 40 days (D–F) and 350 °C, 400 MPa, 20 days (G–I). The monazite from runs with 2M Ca(OH)$_2$ fluid maintain age record of the original Burnet monazite. In contrast, the altered, patchy zoned monazite from experiments with Na$_2$Si$_2$O$_5$ + H$_2$O fluid includes internal domains that preserved the original ages, and domains altered *via* fluid-aided coupled dissolution-reprecipitation leading to disturbance of the Th-U-Pb system.

± 7.3 Ma (350 °C and 200 MPa), and 1084 ± 7.9 Ma (350 °C and 400 MPa). Dark zones with modified compositions yielded scattered single Th-U-total Pb dates in ranges of 375–771 Ma (250 °C and 200 MPa; Fig. 6C), 82–253 Ma (350 °C and 200 MPa; Fig. 6F), and 95–635 Ma (350 °C and 400 MPa; Fig. 6I). These dates significantly differ from the original age of 1072 ± 2.8 Ma, indicating disturbance of the Th-U-Pb system in the presence of Na$_2$Si$_2$O$_5$ + H$_2$O.
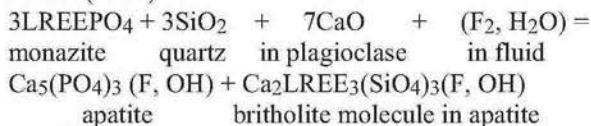
DISCUSSION

Interpretation of experimental results

The experimental results showed significant differences in products between runs with 2M Ca(OH)$_2$ and Na$_2$Si$_2$O$_5$ + H$_2$O fluids. The experiments with 2M Ca(OH)$_2$ were promising with regard to monazite alterations, on the basis of previous experiments with similar starting mineral and fluid composition that resulted in monazite alteration and the formation of a secondary apatite-britholite solid solution and REE-epidote to allanite at 450–500 °C and 450–610 MPa (Budzyń *et al.*, 2011). A high-Ca bulk content of the capsule charge, related to presence of labradorite, CaF$_2$, and 2M Ca(OH)$_2$, was expected to promote the formation of apatite. Experiments also tested whether allanite would

form preferentially at 350 °C and 200–400 MPa, on the basis of thermodynamic modelling of the relative stabilities of monazite and dissakisite-(La), the Mg-equivalent of allanite (Janots *et al.*, 2007), and the stability relations of monazite and allanite (Spear, 2010). However, small amounts of apatite formed only in one experimental run at 350 °C and 400 MPa (M12C-15), but no allanite was formed. The absence of allanite in the products was the outcome least likely to be related to the short duration of experiments. Owing to time limits with respect to natural processes, the fluids were used in excess to increase the reaction rates in the same manner as in the previous experimental study with similar mineral-fluid composition resulting in rapid monazite alteration and allanite growth (Budzyń *et al.*, 2011). The monazite alteration and the formation of allanite were recently reported from experiments in the wide P-T range of 2–10 kbar and 450–750 °C (Budzyń *et al.*, 2014), with similar starting compositions of solids and 2M Ca(OH)$_2$ fluid, as in the present study. The transition between the monazite and allanite stability fields must be located between 350 and 450 °C at 200–400 MPa. The experimental results were consistent with observations from nature that during progressive metamorphism, replacement of monazite by allanite is subsequent to the appearance of biotite (Wing *et al.*, 2003) or, more specifically, occurred at 420–450 °C (Janots *et al.*, 2006, 2008).

The strong alteration of monazite in experiments with $Na_2Si_2O_5 + H_2O$ was consistent with previous experimental work performed at higher P-T conditions (Hetherington *et al.*, 2010; Harlov and Hetherington, 2010; Budzyń *et al.*, 2011; Harlov *et al.*, 2011). The formation of apatite, fluor-britholite-(Ce) or apatite-fluorbritholite-(Ce) solid solution was expected according to the previous experiments of Budzyń *et al.* (2011). Although monazite was partially dissolved in all runs, the apatite- to britholite-group minerals were not stable in the experimental conditions at 250 °C and 200 MPa. REE-enriched apatite to fluorcalciobritholite formed only at 350 °C and 200–400 MPa. The enrichment of the apatite in REE is related to the coupled substitutions of (1) $REE^{3+} + Si^{4+} = Ca^{2+} + P^{5+}$ and (2) $REE^{3+} + Na^+ = 2Ca^{2+}$ (Pan and Fleet, 2002). Concentrations of Si (0.7–5.8 wt % SiO_2; 0.066–0.589 cations per formula unit, c.p.f.u.) and Na (3.7–4.7 wt % Na_2O; 0.723–0.920 c.p.f.u.) are too low to compensate for significant substitution of Y+REE (29.6–37.6 wt % $(Y+REE)_2O_3$; 1.083–1.408 c.p.f.u.; Table 4). This phenomenon can be related to the experimental environment in the capsule that does not completely replicate natural mineral reactions. The simplified reaction, documenting monazite alteration and subsequent REE enrichment in apatite, can be proposed according to Gieré and Sorensen (2004):

$3LREEPO_4 + 3SiO_2 + 7CaO + (F_2, H_2O) =$
monazite   quartz   in plagioclase   in fluid
$Ca_5(PO_4)_3 (F, OH) + Ca_2LREE_3(SiO_4)_3(F, OH)$
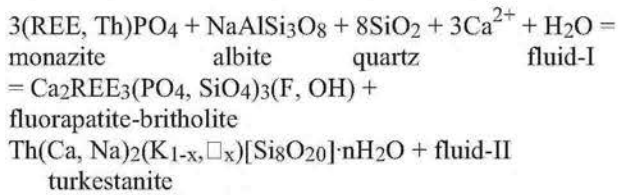   apatite   britholite molecule in apatite

The altered monazite showed porous textures related to partial dissolution. The pores showing preferred orientation along rims (Fig. 3A) or across whole grains (Figs 3C, D, 4) most likely developed owing to alteration, mediated by aggressive F-rich fluid penetrating monazite structure. The elongated pores show an orientation that probably is related to crystallographic parameters. This type of monazite alteration is unknown from previous experiments or in nature. Previous experiments by several authors utilized monazite from a heavy-mineral sand deposit, located in Cleveland County, North Carolina (Hetherington *et al.*, 2010; Budzyń *et al.*, 2011; Harlov *et al.*, 2011; Williams *et al.*, 2011). The experiments with the North Carolina monazite in the presence of a silicate assemblage similar to that of the present study and $Na_2Si_2O_5 + H_2O$ fluid run under P-T conditions of 450–500 °C and 450–610 MPa resulted in the development of patchy zoning related to a fluid-aided coupled dissolution-reprecipitation process (Budzyń *et al.*, 2011; Williams *et al.*, 2011). The altered domains in the North Carolina monazite were depleted in Th, U and Pb with respect to the unaltered patches, representing the composition of the starting monazite. Here, patchy zoning also developed in the altered Burnet monazite. The altered domains were depleted in Y, Th, U, Pb, and Ca, with subsequent enrichment in LREE (Table 2; Fig. 5). The plots of formula proportions REE + P + Y *vs.* Th + U + Si indicated that both the cheralite and huttonite substitutions operated in the original Burnet monazite and the unaltered domains of monazite from experiments (Fig. 5). The huttonite substitution dominated over the cheralite substitution in the altered monazite domains. Although similarities in compositional alteration be-

tween the North Carolina monazite in previous experiments (Budzyń *et al.*, 2011; Williams *et al.*, 2011), and the Burnet monazite in this study, the formation porosity showing preferred orientation in the Burnet monazite is a new type of alteration. Seydoux-Guillaume *et al.* (2012) showed that radiation-damage may facilitate the fluid penetration of monazite, resulting in the remobilization of elements (such as Th, U, Pb) during hydrothermal alteration at temperatures below 320 °C. Here, a high Th concentration (9.4–17.0 wt % ThO_2) and an old age of ca. 1072 Ma may indicate that the Burnet monazite can be affected by radiation damage. Although analyses of the monazite prior to experiments yielded a uniform age with no Th-U-Pb disturbance in the compositional domains, the presence of the metamict sites in the monazite structure cannot be excluded, as evidence of radiation damage was constrained and limited to isolated nannometer-sized domains in the structure (Black *et al.*, 1984; Meldrum *et al.*, 1998; Seydoux-Guillaume *et al.*, 2002b, 2003, 2004, 2007, 2012; Nasdala *et al.*, 2010). Such grains may be more susceptible to preferentially oriented dissolution of monazite during fluid-aided experimental alteration.

Although there was high availability of Ca from CaF_2 and of P from monazite, REE-enriched apatite to fluorcalciobritholite was not the main phase incorporating the Y, REE, Th, and U released during the alteration of monazite in the presence of $Na_2Si_2O_5 + H_2O$. Th, U and REE, were preferentially incorporated into the REE-rich steacyite, which played an important role during the experimental alteration of the monazite. The REE-rich steacyite commonly overgrew the altered monazite, but also filled the pore spaces in altered areas of the monazite. The presence of the REE-rich steacyite inclusions in monazite indicates the fluid-aided transport of Si, Ca, Na, K and other elements into the monazite. The REE-rich steacyite, forming outside of the monazite in the capsule charge, either as intergrowths with monazite or as individual grains, indicates high Th, U and REE mobility, most likely induced by the presence of F in the fluid. The increasing contents of REE and Ca, accompanying increasing experimental P-T conditions, correlate with a decrease in Th and Na, according to the coupled substitution of $REE^{3+} + Ca^{2+} = Th^{4+} + Na^+$ (Vilalva and Vlach, 2010). The presence of individual crystals of REE-enriched apatite to fluorcalciobritholite indicate transport of the Y+REE released from monazite, probably in fluoride complexes, as documented in previous studies on the mobility of Y + REE (Wood, 1990; Pan and Fleet, 1996) or hydroxide complexes (Haas *et al.*, 1995; Poitrasson *et al.*, 2004). A high alkalinity of the fluid induced mobilization of Th (cf. Ermolaeva *et al.*, 2007), promoting further crystallization of individual crystals of REE-rich steacyite.

The previous experiments under conditions of 450–500 °C and 450–610 MPa, using similar mineral composition and $Na_2Si_2O_5 + H_2O$ fluid, documented the alteration of monazite with the formation of a fluorapatite-britholite solid solution and turkestanite, a Th-Ca-Na-K silicate with a similar composition to the REE-rich steacyite of this study, but lower totals indicating the presence of water component (Budzyń *et al.*, 2011). The following reaction presenting the distribution of REE and Th between phosphates and silicates was proposed (Budzyń *et al.*, 2011):

3(REE, Th)PO$_4$ + NaAlSi$_3$O$_8$ + 8SiO$_2$ + 3Ca^{2+} + H$_2$O =
monazite   albite   quartz   fluid-I
= Ca$_2$REE$_3$(PO$_4$, SiO$_4$)$_3$(F, OH) +
fluorapatite-britholite
Th(Ca, Na)$_2$(K$_{1-x}$,□$_x$)[Si$_8$O$_{20}$]·nH$_2$O + fluid-II
    turkestanite

The REE-enriched apatite to fluorcalciobritholite and the REE-rich steacyite formed in this study in accordance with equivalent reactions involving monazite alteration. In nature, the formation of steacyite or turkestanite replacing monazite is probably not documented. Steacyite and turkestanite are known from only several alkaline complexes (e.g., Pautov *et al.*, 1997, 2004; Kabalov *et al.*, 1998; Petersen *et al.*, 1999). In the peralkaline granites of the Morro Redondo Complex in south Brasil, the crystallization of turkestanite, associated britholite and an unnamed (Y-REE)-hydrated silicate was attributed to a post-magmatic stage at temperatures of ca. 450 °C (Vilalva and Vlach, 2010). The current experimental study, partially replicating natural observations, adds important new data to our knowledge of the partitioning of Th, U and REE between phosphates and silicates under conditions of 250–350 °C, replicating post-magmatic, low-temperature hydrothermal processes in a high-alkali- and alkaline environment.

Implications for the natural occurrence of monazite and Th-U-Pb geochronology

The experimental results add important information to the limited knowledge on the stability of monazite in low-temperature processes. The alteration of monazite and the formation of Th-silicates was also recognized in hydrothermally altered granitic rocks in the Precambrian crystalline basement of the Athabasca Basin, Saskatchewan, Canada (Hecht and Cuney, 2000). Poitrasson *et al.* (2000) also reported alteration in hydrothermally altered Palaeozoic granites in the Massif Central (France), Cornwall (England) and the Lake District (England) under temperature conditions of ca. 260–340 °C, affecting monazite *via* coupled dissolution-reprecipitation, resulting in cationic substitutions and selective Th depletion. The alteration of detrital igneous monazite under mid-greenschist facies conditions (ca. 350 °C), resulted in replacement by low-Th metamorphic monazite, apatite and ThSiO$_4$ in sandstones with a low-Ca bulk composition, or allanite in moderate- to high-Ca sandstones in the Witwatersrand basin, South Africa (Rasmussen and Muhling, 2009). Also, Rasmussen and Muhling (2007) reported monazite with high-Th cores and low-Th rims with ThSiO$_4$ inclusions in metasedimentary rocks from the Paleoproterozoic Stirling Range Formation (southwestern Australia). The presence of low-Th, inclusion-rich rims was interpreted as being related to the replacement of older monazite *via* a dissolution and reprecipitation process under conditions of low-grade metamorphism (<400 °C; Rasmussen and Muhling, 2007). The results of the study reported here show that monazite remains stable in experiments replicating low-grade metamorphic conditions in high bulk Ca composition of the capsule charge (runs with 2M Ca(OH)$_2$ fluid). On the other hand, the experiments with elevated bulk contents of

Na and Ca, related to the presence of Na$_2$Si$_2$O$_5$ + H$_2$O and CaF$_2$ in excess, respectively, have shown that monazite is unstable in this kind of bulk composition. Remobilized Th and U were incorporated in a newly formed REE-rich steacyite, The Th-rich phase that was apparently stable in the alkaline system used, in contrast to ThSiO$_4$ formed during low-temperature monazite alteration in nature, mentioned above. It should be also noted that compositional alteration during the experiments included LREE-enrichment and HREE-depletion of the altered domains in monazite (Table 2).

Previous experiments showed that the fluid-mediated coupled dissolution-reprecipitation process may result in selective remobilization of Th, U and Pb in monazite, significantly affecting the age record in high-grade rocks (Teufel and Heinrich, 1997; Seudoux-Guillaume *et al.*, 2002a; Harlov *et al.*, 2007, 2011; Harlov and Hetherington 2010; Hetherington *et al.*, 2010). The essential "dating" of experimental products from runs under P-T conditions of 450 MPa and 450 °C over 16 days showed that altered zones in patchy monazite (the starting monazite was homogeneous) yielded an "age" of nearly zero, while unaltered domains maintain the age of ca. 350 Ma of the North Caroline monazite used in the experiments (Williams *et al.*, 2011). The study by the present authors used a similar starting mineral assemblage in the presence of Na$_2$Si$_2$O$_5$ + H$_2$O fluid, as used in Williams *et al.* (2011). The recorded Th-U-total Pb age disturbance in the altered domains did not result in the complete resetting of the Th-U-Pb clock, but rejuvenated the "ages" of monazite internal domains from 1072 ± 2.8 Ma to 375–771 Ma (250 °C, 200 MPa), 82–253 Ma (350 °C, 200 MPa), and 95–635 Ma (350 °C, 400 MPa). The possibility cannot be excluded that low-temperature metamorphic conditions are too low to reset the monazite clock. There are several factors that may control and limit the alteration mechanism. It should be noted, that the Au capsule forms a closed system of solids and fluid and fluid reactivity decreases with time during the experiment. The low P-T conditions were compensated by durations of 40 and 20 days in 250 °C and 350 °C runs, respectively, compared to the 16 days used in Williams *et al.* (2011). The "age" record, reflecting a disturbance of the Th-U-Pb system in the altered domains (Fig. 6C, F, I), is strictly related to the rate of remobilization of these elements. The mechanism of monazite alteration *via* fluid-mediated coupled dissolution-reprecipitation in the experiments is probably limited remobilization of the elements. Therefore, a crucial factor most likely is the composition of the Burnet monazite, containing 0.5–0.9 wt % PbO in contrast to the significantly lower amounts of 0.10–0.16 wt % PbO in the North Caroline monazite. The high Pb content explains partial instead of complete removal of Pb in the altered domains of the Burnet monazite. Future experiments should expand the considerations of timing to constrain the effects of experiment duration on the remobilization of the elements in monazite structure under low-temperature conditions.

The potentially altered compositional domains of monazite may be reflected in the dark patches in high-contrast BSE imaging, the presence of secondary minerals inclusions or the porosity developed. Assuming a total removal of Pb, monazite can provide an age record of the metaso-

matic event (Williams *et al.*, 2011). However, the low-temperature alteration may result in the disturbance of the Th-U-Pb system of monazite without complete resetting the ages, as shown in the present study. For instance, the post-magmatic alteration of granitic rocks is very common and avoiding altered domains may provide accurate geochronological data, as in the case of the Stolpen granite with recognized postmagmatic monazite alteration (Lisowiec *et al.*, 2013), where further study involving monazite dating provided the age of the magmatic event and the emplacement of the granitoid pluton (Lisowiec *et al.*, 2014). The recognition of the monazite domains affected by fluid-mediated alteration is crucial in applications of monazite geochronology.

CONCLUSIONS

This experimental study provides important data for the understanding and interpretation of metasomatic processes in nature.

1) Monazite is stable under conditions of 250–350 °C and 200–400 MPa in the presence of 2M $Ca(OH)_2$ fluid. Lack of allanite in the experimental products is related to the monazite-to-allanite transition at higher P-T conditions.

2) A system high in Na-Ca with a $Na_2Si_2O_5 + H_2O$ fluid promotes monazite alteration. Released REE, Th and U are incorporated in newly formed REE-enriched apatite, fluorcalciobritholite and REE-rich steacyite. The predominance of the REE-rich steacyite in the products indicates preferential partitioning of Th and REE in silicates over phosphates during processes at 250–350 °C.

3) Partial removal of Pb from the monazite used in the experiments resulted in the disturbance of the Th-U-Pb system without complete resetting of the monazite clock. Monazite geochronological data from natural samples should be interpreted with caution. This is also true for the correlation of compositional, textural and age data to understand the effects of the recorded processes on monazite composition and potentially the ages recorded.

REFERENCES

Aleinikoff, J. N., Grauch, R. I., Mazdab, F. K., Kwak, L., Fanning, C. M. & Kamo, S. L., 2012. Origin of an unusual monazite-xenotime gneiss, Hudson Highlands, New York: SHRIMP U-Pb geochronology and trace element geochemistry. *American Journal of Science*, 312: 723–765.

Appel, P., Cirrincione, R., Fiannacca, P. & Pezzino, A., 2011. Age constraints on Late Paleozoic evolution of continental crust from electron microprobe dating of monazite in the Peloritani Mountains (southern Italy): another example of resetting of monazite ages in high-grade rocks. *International Journal of Earth Sciences (Geologische Rundschau)*, 100: 107–123.

Ayers, J. C., Crombie, S., Loflin, M., Miller, C. F. & Luo, Y., 2013. Country rock monazite response to intrusion of the Searchlight pluton, Southern Nevada. *American Journal of Science*, 313: 345–394.

Black, L. P., Fitzgerald, J. D. & Harley, S. L., 1984. Pb isotopic composition, colour, and microstructure of monazites from a polymetamorphic rock in Antarctica. *Contributions to Mineralogy and Petrology*, 85: 141–148.

Broska, I. & Siman, P., 1998. The breakdown of monazite in the West-Carpathian Veporic orthogneisses and Tatric granites. *Geologica Carpathica*, 49: 161–167.

Broska, I., Williams, C. T., Janák, M. & Nagy, G., 2005. Alteration and breakdown of xenotime-(Y) and monazite-(Ce) in granitic rocks of the Western Carpathians, Slovakia. *Lithos*, 82: 71–83.

Budzyń, B., Harlov, D. E., Majka, J. & Kozub, G. A., 2014. Experimental constraints on the monazite-fluorapatite-allanite and xenotime-(Y,HREE)-rich fluorapatite-(Y,HREE)-rich epidote phase relations as a function of pressure, temperature, and Ca vs. Na activity in the fluid. *Geophysical Research Abstracts*, 16, EGU2014–8583.

Budzyń, B., Harlov, D. E., Williams, M. L. & Jercinovic, M. J., 2011. Experimental determination of stability relations between monazite, fluorapatite, allanite, and REE-epidote as a function of pressure, temperature, and fluid composition. *American Mineralogist*, 96: 1547–1567.

Budzyń, B., Hetherington, C. J., Williams, M. L., Jercinovic, M. J. & Michalik, M., 2010. Fluid-mineral interactions and constraints on monazite alterations during metamorphism. *Mineralogical Magazine*, 74: 633–655.

Budzyń, B. & Kozub-Budzyń, G. A., 2015. The stability of xenotime in high Ca and Ca-Na systems under experimental conditions of 250–350 °C and 200–400 MPa: the implications for fluid-mediated low-temperature processes in granitic rocks. *Geological Quarterly*, 59: (in press). DOI: 10.7306/gq.1223.

Cherniak, D. J. & Pyle, J. M., 2008. Th diffusion in monazite. *Chemical Geology*, 256: 52–61.

Cherniak, D. J., Watson, E. B., Grove, M. & Harrison, T. M., 2004. Pb diffusion in monazite: a combined RBS/SIMS study. *Geochimica et Cosmochimica Acta*, 68: 829–840.

Cuney, M. & Mathieu, R., 2000. Extreme light rare element mobilization by diagenetic fluids in the geological environment of the Oklo natural reactor zones, Franceville basin, Gabon. *Geology*, 28: 743–746.

Ermolaeva, V. N., Pekov, I. V., Chukanov, N. V. & Zadov, A. E., 2007. Thorium mineralization in hyperalkaline pegmatites and hydrothermalites of the Lovozero Pluton, Kola Peninsula. *Geology of Ore Deposits*, 49: 758–775.

Finger, F., Broska, I., Roberts, M. P. & Schermaier, A., 1998. Replacement of primary monazite by apatite-allanite-epidote coronas in an amphibolite facies granite gneiss from the eastern Alps. *American Mineralogist*, 83: 248–258.

Förster, H.-J., 1998. The chemical composition of REE-Y-Th-U-rich accessory minerals in peraluminous granites of the Erzgebirge-Fichtelgebirge region, Germany, Part I: The monazite-(Ce)-brabantite solid solution series. *American Mineralogist*, 83: 259–272.

Gardes, E., Jaoul, O., Montel, J., Seydoux-Guillaume, A. M. &

Wirth, R., 2006. Pb diffusion in monazite: an experimental study of $Pb^{2+} + Th^{4+}$ $2Nd^{3+}$ interdiffusion. *Geochimica et Cosmochimica Acta*, 70: 2325–2336.

Gieré, R. & Sorensen, S. S., 2004. Allanite and other REE-rich epidote-group minerals. In: Liebscher, A. & Franz, G. (eds), *Epidotes. Reviews in Mineralogy and Geochemistry*. The Mineralogical Society of America, Washington, DC, U.S.A., 56: 431–493.

Haas, J. R., Shock, E. L. & Sassani, D. C., 1995. Rare earth element in hydrothermal systems: Estimates of standard partial molal thermodynamic properties of aqueous complexes of the rare earth elements at high pressures and temperatures. *Geochimica et Cosmochimica Acta*, 59: 4329–4350.

Harlov, D. E. & Hetherington, C. J., 2010. Partial high-grade alteration of monazite using alkali-bearing fluids: Experiment and nature. *American Mineralogist*, 95: 1105–1108.

Harlov, D. E., Wirth, R. & Hetherington, C. J., 2007. The relative stability of monazite and huttonite at 300–900°C and 200–1000 MPa: metasomatism and the propagation of metastable mineral phases. American Mineralogist, 92: 1652–1664.

Harlov, D. E., Wirth, R. & Hetherington, C. J., 2011. Fluid-mediated partial alteration in monazite: the role of coupled dissolution-reprecipitation in element redistribution and mass transfer. *Contributions to Mineralogy and Petrology*, 162: 329– 348.

Hecht, L. & Cuney, M., 2000. Hydrothermal alteration of monazite in the Precambrian crystalline basement of the Athabasca Basin (Saskatchewan, Canada): implications for the formation of unconformity-related uranium deposits. *Mineralium Deposita*, 35: 791–795.

Hetherington, C. J., Harlov, D. E. & Budzyń, B., 2010. Experimental initiation of dissolution-reprecipitation reactions in monazite and xenotime: the role of fluid composition. *Mineralogy and Petrology*, 99: 165–184.

Janots, E., Brunet, F., Goffé, B., Poinssot, C., Burchard, M. & Cemic, L., 2007. Thermochemistry of monazite-(La) and dissakisite-(La): implications for monazite and allanite stability in metapelites. *Contributions to Mineralogy and Petrology*, 154: 1–14.

Janots, E., Engi, M., Berger, A., Allaz, J., Schwarz, J.-O. & Spandler, C., 2008. Prograde metamorphic sequence of REE minerals in pelitic rocks of the Central Alps: implications for allanite-monazite-xenotime phase relations from 250 to 610°C. *Journal of Metamorphic Geology*, 26: 509–526.

Janots, E., Negro, F., Brunet, F., Goffé, B., Engi, M. & Bouybaouene, M. L., 2006. Evolution of the REE mineralogy in HP-LT metapelites of the Sebtide complex, Rif, Morocco: monazite stability and geochronology. *Lithos*, 87: 214–234.

Jercinovic, M. J. & Williams, M. L., 2005. Analytical perils (and progress) in electron microprobe trace element analysis applied to geochronology: Background acquisition, interferences, and Beam Irradiation Effects. *American Mineralogist*, 90: 526–246.

Jercinovic, M. J., Williams, M. L. & Lane, E. D., 2008. In situ trace element analysis in complex, multi-phase materials by EPMA. *Chemical Geology*, 254: 197–215.

Kabalov, Yu. K., Sokolova, E. V., Pautov, L. A. & Schneider, J., 1998. Crystal structure of a new mineral turkestanite: a calcium analogue of steacyite. *Crystallography Reports*, 43: 584–588. [Translated from Russian in: Kristallografiya, 43, 4: 632–636.]

Konečný, P., Siman, P., Holický, I., Janák, M. & Kollárová, V., 2004. Method of monazite dating by means of the electron microprobe. *Mineralogia Slovaca*, 36: 225–235 [In Slovak, with English abstract].

Lee, D. E. & Bastron, H., 1967. Fractionation of rare-earth ele-

ments in allanite and monazite as related to geology of the Mt. Wheeler mine area, Nevada. *Geochimica et Cosmochimica Acta*, 31: 339–356.

Lee, D. E. & Dodge, F. C. W., 1964. Accessory minerals in some granitic rocks in California and Nevada as a function of calcium content. *American Mineralogist*, 49: 1660–1669.

Linthout, K., 2007. Tripartite division of the system $2REEPO_4$ – $CaTh(PO_4)_2$ – $2ThSiO_4$, discreditation of brabantite, and recognition of cheralite as the name for members dominated by $CaTh(PO_4)_2$. *Canadian Mineralogist*, 45: 503–508.

Lisowiec, K., Budzyń, B., Słaby, E., Renno, A. D. & Götze, J., 2013. Fluid-induced magmatic and post-magmatic zircon and monazite patterns in granitoid pluton and related rhyolitic bodies. *Chemie der Erde – Geochemistry*, 73: 163–179.

Lisowiec, K., Budzyń, B., Słaby, E., Schulz, B. & Renno, A. D., 2014. Th-U-total Pb timing constraints on the emplacement of the granitoid pluton of Stolpen, Germany. *Acta Geologica Polonica*, 64: 457–472.

Majka, J. & Budzyń, B., 2006. Monazite breakdown in metapelites from Wedel Jarlsberg Land, Svalbard – preliminary results. *Mineralogia Polonica*, 37: 61–69.

Meldrum, A., Boatner, L. A., Weber, W. J. & Ewing, R. C., 1998. Radiation damage in zircon and monazite. *Geochimica et Cosmochimica Acta*, 62: 2509–2520.

Montel, J. M., Foret, S., Veschambre, M., Nicollet, C. & Provost, A., 1996. Electron microprobe dating of monazite. *Chemical Geology*, 131: 37–53.

Nasdala, L., Ruschel, K., Rhede, D., Wirth, R., Kerschhofer-Wallner, L., Kennedy, A. K., Kinny, P. D., Finger, F. & Groschopf, N., 2010. Phase decomposition upon alteration of radiation damaged monazite-(Ce) from Moss, Řstfold, Norway. *Chimia*, 64: 705–711.

Ondrejka, M., Uher, P., Putiš, M., Broska, I., Bačík, P., Konečný, P. & Schmiedt, I., 2012. Two-stage breakdown of monazite by post-magmatic and metamorphic fluids: An example from the Veporic orthogneiss, Western Carpathians, Slovakia. *Lithos*, 142–142: 245–255.

Pan, Y. & Fleet, M. E., 1996. Rare earth element mobility during prograde granulite facies metamorphism: significance of fluorine. *Contributions to Mineralogy and Petrology*, 123: 251–262.

Pan, Y. & Fleet, M. E., 2002. Composition of the apatite-group minerals: substitution mechanisms and controlling factors. In: Kohn, M. J., Rakovan, J. & Hughes, J. M. (eds) *Phosphates: Geochemical, Geobiological, and Materials Importance. Reviews in Mineralogy and Geochemistry*, 48: 13–49.

Parrish, R. R., 1990. U-Pb dating of monazite and its application to geological problems. *Canadian Journal of Earth Sciences*, 27: 1431–1450.

Pautov, L.A., Agakhanov, A.A., Sokolova, E. & Hawthorne, F.C., 2004. Maleevite, $BaB_2Si_2O_8$, and pekovite, $SrB_2Si_2O_8$, new mineral species from the Dara-i-Pioz alkaline massif, Northern Tajikistan: description and crystal structure. *The Canadian Mineralogist*, 42: 107–119.

Pautov, L.A., Agakhanov, A.A., Sokolova, E.V. & Kabalov, Yu. K., 1997. Turkestanite $–Th(Ca,Na)_2(K_{1-x}, \square_x)(Si_8O_{20})$ nH_2O: A new mineral with Si-O rings. *Zapiski Vserossiyskogo Mineralogicheskogo Obshchestva*, 126: 45–55.

Petersen, O. V., Johnsen, O. & Micheelsen, H. I., 1999. Turkestanite from the Ilímaussaq alkaline complex, South Greenland. *Neues Jahrbuch für Mineralogie, Monatshefte*, 9: 424–432.

Petrík, I. & Konečný, P., 2009. Metasomatic replacement of inherited metamorphic monazite in a biotite-garnet granite from the Nízke Tatry Mountains, Western Carpathians, Slovakia:

Chemical dating and evidence for disequilibrium melting. *American Mineralogist*, 94: 957–974.

Poitrasson, F., Chenery, S. & Bland, D. J., 1996. Contrasted monazite hydrothermal alteration mechanisms and their geochemical implications. *Earth and Planetary Science Letters*, 145: 79–96.

Poitrasson, F., Chenery, S. & Shepherd, T. J., 2000. Electron microprobe and LA-ICPMS study of monazite hydrothermal alteration; implications for U-Th-Pb geochronology and nuclear ceramics. *Geochimica et Cosmochimica Acta*, 64: 3283–3297.

Poitrasson, F., Oelkers, E., Schott, J. & Montel, J.-M., 2004. Experimental determination of synthetic $NdPO_4$ monazite end-member solubility in water from 21 to 300°C: implications for rare earth element mobility in crustal fluids. *Geochimica et Cosmochimica Acta*, 68: 2207–2221.

Pyle, J. M., Spear, F. S., Wark, D. A., Daniel, Ch. D. & Storm, L. C., 2005. Contributions to precision and accuracy of monazite microprobe ages. *American Mineralogist*, 90, 547–577.

Rasmussen, B. & Muhling, J. R., 2007. Monazite begets monazite: evidence for the dissolution of detrital monazite and reprecipitation of syntectonic monazite during low-grade regional metamorphism. *Contributions to Mineralogy and Petrology*, 154: 675–689.

Rasmussen, B. & Muhling, J. R., 2009. Reactions destroying detrital monazite in greenschist-facies sandstones from the Witwatersrand basin, South Africa. *Chemical Geology*, 264: 311–327.

Read, D., Andreoli, M. A. G., Knoper, M., Williams, C. T. & Jarvis, N., 2002. The degradation of monazite: Implications for the mobility of rare-earth and actinide elements during low-temperature alteration. *European Journal of Mineralogy*, 14: 487–498.

Ruschel, K., Nasdala, L., Kronz, A., Hanchar, J. M., Többens, D. M., Škoda, R., Finger, F., Möller, A., 2012. A Raman spectroscopic study on the structural disorder of monazite-(Ce). *Mineralogy and Petrology*, 105: 41–55.

Seydoux-Guillaume, A. M., Goncalves, P., Wirth, R. & Deutsch, A., 2003. TEM study of polyphasic and discordant monazites: site specific specimen preparation using the Focused Ion Beam technique. *Geology*, 31: 973–976.

Seydoux-Guillaume, A.-M., Montel, J.-M., Bingen, B., Bosse, V., de Parseval, P., Paquette, J.-L., Janots, E. & Wirth, R., 2012. Low-temperature alteration of monazite: Fluid mediated coupled dissolution-precipitation, irradiation damage, and disturbance of the U-Pb and Th-Pb chronometers. *Chemical Geology*, 330–331: 140–158.

Seydoux-Guillaume, A. M., Paquette, J. L., Wiedenbeck, M., Montel, J. M. & Heinrich, W., 2002a. Experimental resetting of the U-Th-Pb systems in monazite. *Chemical Geology*, 191: 165–181.

Seydoux-Guillaume, A. M., Wirth, R., Deutsch, A. & Schärer, U., 2004. Microstructure of 24–1928 Ma concordant monazites: implications for geochronology and nuclear waste deposits. *Geochimica et Cosmochimica Acta*, 68: 2517–2527.

Seydoux-Guillaume, A. M., Wirth, R. & Ingrin, J., 2007. Contrasting response of $ThSiO_4$ and monazite to natural irradiation. *European Journal of Mineralogy*, 19: 7–14.

Seydoux-Guillaume, A. M., Wirth, R., Nasdala, L., Gottschalk,

M., Montel, J. M. & Heinrich, W., 2002b. An XRD, TEM and Raman study of experimentally annealed natural monazite. *Physics and Chemistry of Minerals*, 29: 240–253.

Spear, F. S., 2010. Monazite–allanite phase relations in metapelites. *Chemical Geology*, 279: 55–62.

Spear, F. S., Pyle, J. M. & Cherniak, D., 2009. Limitations of chemical dating of monazite. *Chemical Geology*, 266: 227–239.

Suzuki, K. & Adachi, M., 1991. Precambrian provenance and Silurian metamorphism of the Tsubonosawa paragneiss in the South Kitakami terrane, Northeast Japan, revealed by the chemical Th-U-total Pb isochron ages of monazite, zircon, and xenotime. *Geochemical Journal*, 25: 357–376.

Suzuki, K. & Kato, T., 2008. CHIME dating of monazite, xenotime, zircon and polycrase: Protocol, pitfalls and chemical criterion of possibly discordant age data. *Gondwana Research*, 14, 569–586.

Tartèse, R., Ruffet, G., Poujol, M., Boulvais, P. & Ireland, T. R., 2011. Simultanous resetting of the muscovite K-Ar and monazite U-Pb geochronometers: a story of fluids. *Terra Nova*, 23: 390–398.

Teufel, S. & Heinrich, W., 1997. Partial resetting of the U-Pb isotope system in monazite through hydrothermal experiments: An SEM and U-Pb isotope study. *Chemical Geology*, 137: 273–281.

Townsend, K. J., Miller, C. F., D'Andrea, J. L., Ayers, J. C., Harrison, T. M. & Coath, C. D., 2000. Low temperature replacement of monazite in the Ireteba granite, Southern Nevada: geochronological implications. *Chemical Geology*, 172: 95–112.

Vilalva, F. C. J. & Vlach, S. R. F., 2010. Major- and trace-element composition of REE-rich turkestanite from peralkaline granites of the Morro Redondo Complex, Graciosa Province, south Brasil. *Mineralogical Magazine*, 74: 645–658.

Vozárová, A., Konečný, P., Šarinová, K. & Vozár, J., 2014. Ordovician and Cretaceous tectonothermal history of the Southern Gemericum Unit from microprobe monazite geochronology (Western Carpathians, Slovakia). *International Journal of Earth Sciences (Geologische Rundschau)*, 103: 1005–1022.

Williams, M. L. & Jercinovic, M. J., 2002. Microprobe monazite geochronology: putting absolute time into microstructural analyses. *Journal of Structural Geology*, 24: 1013–1028.

Williams, M. L., Jercinovic, M. J., Harlov, D. E., Budzyń, B. & Hetherington, C. J., 2011. Resetting monazite ages during fluid-related alteration. *Chemical Geology*, 283: 218–225.

Williams, M. L., Jercinovic, M. J. & Hetherington, C. J., 2007. Microprobe monazite geochronology: understanding geologic processes by integrating composition and chronology. *Annual Review of Earth and Planetary Sciences*, 35: 137–175.

Wing, B. A., Ferry, J. M. & Harrison, T. M., 2003. Prograde destruction and formation of monazite and allanite during contact and regional metamorphism of pelites: petrology and geochronology. *Contributions to Mineralogy and Petrology*, 145: 228–250.

Wood, S. A., 1990. The aqueous geochemistry of the rare earth elements and yttrium: 1. Review of available low-temperature data for inorganic complexes and the inorganic REE speciation of natural waters. *Chemical Geology*, 82: 159–186.

Appendix 1. Average results of the electron microprobe analyzes of labradorite, albite and K-feldspar

Sample	T [°C]	P [MPa]	duration [days]	n	SiO$_2$	Al$_2$O$_3$	MgO	CaO	FeO	SrO	BaO	Na$_2$O	K$_2$O	Total
Starting labradorite				14	52.54	29.10	0.09	12.14	0.34	0.11	<0.01	4.34	0.26	98.92
					0.74	*0.52*	*0.02*	*0.10*	*0.03*	*0.05*		*0.13*	*0.01*	
M12C-04	250	200	40	5	53.60	29.26	0.10	12.21	0.35	0.13	<0.01	4.31	0.27	100.23
					0.26	*0.13*	*0.02*	*0.06*	*0.01*	*0.03*		*0.04*	*0.02*	
M12C-05	350	200	40	5	52.21	28.91	0.08	12.28	0.34	0.11	0.03	4.17	0.27	98.39
					0.11	*0.13*	*0.02*	*0.05*	*0.04*	*0.02*	*0.00*	*0.07*	*0.01*	
M12C-15	350	400	20	2	53.52	29.62	0.10	12.12	0.30	0.13	0.02	4.27	0.20	100.29
					0.42	*0.27*	*0.01*	*0.07*	*0.01*	*0.03*	*0.01*	*0.07*	*0.07*	
Starting albite				10	68.77	19.74	<0.01	0.02	<0.01	0.03	<0.01	11.77	0.05	100.40
					0.49	*0.21*		*0.03*		*0.04*		*0.19*	*0.02*	
M12N-04	250	200	40	5	69.57	19.41	<0.01	0.03	0.03	<0.01	<0.01	11.43	0.07	100.54
					0.30	*0.13*		*0.01*	*0.01*			*0.15*	*0.01*	
M12N-05	350	200	40	4	68.14	19.25	<0.01	0.05	0.06	<0.01	<0.01	11.29	0.07	98.86
					0.26	*0.09*		*0.02*	*0.04*			*0.06*	*0.01*	
M12N-15	350	400	20	5	65.09	18.81	<0.01	<0.01	0.14	0.15	0.94	1.54	13.31	100.00
					0.39	*0.11*			*0.01*	*0.07*	*0.04*	*0.03*	*0.72*	
Starting K-feldspar				23	64.10	18.72	<0.01	<0.01	0.13	0.16	0.94	1.56	13.80	99.43
					0.62	*0.20*			*0.03*	*0.06*	*0.05*	*0.07*	*0.29*	
M12C-04	250	200	40	5	64.91	18.51	<0.01	0.02	0.17	<0.01	0.97	1.53	14.07	100.17
					0.27	*0.10*		*0.00*	*0.02*		*0.02*	*0.04*	*0.07*	
M12C-05	350	200	40	5	60.51	20.91	<0.01	6.08	0.19	0.15	0.97	1.99	10.60	101.40
					5.54	*5.10*		*8.57*	*0.10*	*0.03*	*0.02*	*1.17*	*6.89*	
M12C-15	350	400	20	10	65.32	18.83	<0.01	<0.01	0.14	0.17	0.95	1.50	13.28	100.21
					0.37	*0.07*			*0.03*	*0.04*	*0.04*	*0.07*	*0.73*	
M12N-04 unaltered	250	200	40	11	64.59	18.72	<0.01	<0.01	0.14	0.13	0.95	1.55	13.86	99.94
					0.33	*0.23*			*0.02*	*0.06*	*0.04*	*0.04*	*0.24*	
M12N-04 altered rim				2	68.98	19.08	<0.01	0.03	0.05	<0.01	<0.01	11.22	0.21	99.57
					0.88	*0.08*		*0.01*	*0.02*			*0.27*	*0.15*	
M12N-05 unaltered	350	200	40	8	64.18	18.69	<0.01	<0.01	0.16	0.14	0.91	1.57	13.88	99.53
					1.29	*0.49*			*0.03*	*0.03*	*0.05*	*0.08*	*0.15*	
M12N-05 altered rim				3	69.57	19.16	<0.01	<0.01	0.19	<0.01	<0.01	11.51	0.21	100.66
					0.75	*0.19*			*0.02*			*0.28*	*0.11*	
M12N-15 unaltered	350	400	20	6	65.02	18.47	<0.01	0.20	0.17	0.07	0.51	1.32	14.39	100.13
					1.34	*0.55*		*0.40*	*0.09*	*0.06*	*0.46*	*0.37*	*0.58*	
M12N-15 altered rim				4	69.28	19.42	<0.01	0.05	0.19	<0.01	<0.01	11.42	0.22	100.60
					0.62	*0.58*		*0.03*	*0.13*			*0.16*	*0.06*	

Comments: all values are given in wt %; *italic* – standard deviation.

Appendix 2. Average results of the electron microprobe analyzes of biotite and muscovite

Sample	T [°C]	P [MPa]	dura-tion [days]	n	SiO$_2$	TiO$_2$	Al$_2$O$_3$	Cr$_2$O$_3$	MgO	CaO	MnO	FeO	NiO	Na$_2$O	K$_2$O	F	Cl	Total
Starting biotite				24	34.77	3.75	18.56	0.06	9.23	<0.01	0.03	16.95	0.02	0.08	9.16	0.20	<0.01	92.84
					0.45	*0.70*	*0.62*	*0.04*	*0.56*		*0.02*	*0.53*	*0.02*	*0.02*	*0.09*	*0.11*		
M12C-04	250	200	40	5	35.47	4.36	18.48	0.07	8.91	0.05	0.05	17.15	<0.01	0.08	9.42	0.11	<0.01	94.11
					0.16	*0.34*	*0.22*	*0.01*	*0.51*	*0.05*	*0.03*	*0.69*		*0.03*	*0.12*	*0.09*		
M12C-05	350	200	40	5	34.88	4.44	17.99	0.07	8.77	0.05	0.05	17.51	<0.01	0.09	9.39	0.09	<0.01	93.28
					0.24	*0.55*	*0.38*	*0.01*	*0.30*	*0.02*	*0.01*	*0.93*		*0.04*	*0.09*	*0.07*		

Sample	T [°C]	P [MPa]	dura-tion [days]	n	SiO$_2$	TiO$_2$	Al$_2$O$_3$	Cr$_2$O$_3$	MgO	CaO	MnO	FeO	NiO	Na$_2$O	K$_2$O	F	Cl	Total
M12C-15	350	400	20	5	35.44	4.65	18.39	0.05	8.62	0.02	0.04	17.00	0.03	0.09	9.32	0.16	<0.01	93.80
					0.52	*0.12*	*0.28*	*0.01*	*0.28*	*0.02*	*0.02*	*0.43*	*0.02*	*0.01*	*0.09*	*0.10*		
M12N-04	250	200	40	5	35.64	4.54	18.39	0.06	9.01	0.03	0.06	17.63	0.02	0.10	9.46	0.17	<0.01	95.03
					0.41	*0.15*	*0.42*	*0.03*	*0.35*	*0.03*	*0.02*	*0.66*	*0.02*	*0.02*	*0.13*	*0.07*		
M12N-05	350	200	40	5	34.82	4.54	17.88	0.06	8.96	0.02	0.05	17.69	0.02	0.12	9.56	0.12	<0.01	93.79
					0.41	*0.37*	*0.42*	*0.03*	*0.38*	*0.02*	*0.02*	*0.28*	*0.02*	*0.03*	*0.07*	*0.05*		
M12N-15	350	400	20	6	36.04	4.16	18.47	0.03	8.87	0.03	0.03	16.89	0.02	0.24	9.29	0.17	<0.01	94.25
					0.39	*0.65*	*0.16*	*0.01*	*0.19*	*0.03*	*0.03*	*0.11*	*0.03*	*0.24*	*0.15*	*0.15*		
Starting muscovite				12	46.56	0.17	34.10	<0.01	0.91	<0.01	0.07	2.46	<0.01	0.65	9.65	<0.01	<0.01	94.58
					0.53	*0.06*	*0.75*		*0.27*		*0.03*	*0.35*		*0.09*	*0.19*		
M12C-04	250	200	40	4	45.58	0.18	33.37	<0.01	0.99	0.04	0.07	2.57	0.02	0.69	10.06	<0.01	<0.01	93.57
					0.12	*0.06*	*0.27*		*0.12*	*0.01*	*0.04*	*0.08*	*0.02*	*0.05*	*0.07*		
M12C-05	350	200	40	5	45.23	0.15	33.41	0.02	1.01	0.04	0.07	2.82	<0.01	0.66	9.95	<0.01	<0.01	93.37
					0.21	*0.03*	*0.15*	*0.02*	*0.13*	*0.03*	*0.04*	*0.08*		*0.04*	*0.16*		
M12C-15	350	400	20	5	49.14	0.15	35.52	<0.01	1.02	0.04	0.04	2.66	<0.01	0.50	8.80	<0.01	<0.01	97.86
					0.36	*0.03*	*0.10*		*0.08*	*0.03*	*0.03*	*0.11*		*0.13*	*0.17*		
M12N-04	250	200	40	5	45.76	0.15	33.49	<0.01	1.02	0.07	0.05	2.66	<0.01	0.77	10.06	<0.01	<0.01	94.03
					0.76	*0.04*	*0.50*		*0.06*	*0.09*	*0.06*	*0.07*		*0.11*	*0.13*		
M12N-05	350	200	40	5	45.28	0.17	32.90	<0.01	1.16	0.03	0.06	2.89	<0.01	0.71	10.03	<0.01	<0.01	93.24
					0.13	*0.03*	*0.26*		*0.17*	*0.01*	*0.02*	*0.23*		*0.02*	*0.10*		
M12N-15	350	400	20	5	48.71	0.14	35.03	0.03	1.07	0.03	0.07	2.68	0.02	0.75	8.84	0.04	<0.01	97.39
					0.40	*0.05*	*0.69*	*0.02*	*0.02*	*0.03*	*0.03*	*0.07*	*0.02*	*0.10*	*0.30*	*0.04*		

Comments: all values are given in wt %; Total values are corrected for O = F; *Italic* – standard deviation.

Appendix. 3. Results of electron microprobe analyzes of monazite presenting contents of Th, U, Pb and Y, calculated Th* and monazite Th-U-total Pb ages

Analysis	Th [wt %]	±2σ	U [wt %]	±2σ	Pb [wt %]	±2σ	Y [wt %]	Th* [wt %]	Age [Ma]	±1σ
Unaltered; Average age ±2σ = 1095±4.6 Ma; MSWD = 1.74										
M12C-04_1-1	10.0927	0.0447	0.2972	0.0127	0.5537	0.0075	0.6776	11.12	1093	20.7
M12C-04_1-2	10.5048	0.0458	0.3232	0.0130	0.5711	0.0076	0.7084	11.62	1079	20.0
M12C-04_1-3	10.3333	0.0454	0.3165	0.0129	0.5700	0.0076	0.6749	11.43	1095	20.3
M12C-04_1-4	10.3311	0.0454	0.3067	0.0129	0.5664	0.0076	0.6994	11.39	1092	20.4
M12C-04_1-5	10.3897	0.0455	0.3119	0.0129	0.5676	0.0076	0.6924	11.47	1087	20.2
M12C-04_2-1	8.9550	0.0421	0.2913	0.0127	0.4886	0.0073	0.4947	9.96	1078	22.2
M12C-04_2-2	8.8491	0.0420	0.2832	0.0127	0.4875	0.0073	0.4729	9.83	1089	22.6
M12C-04_2-3	8.9498	0.0423	0.2831	0.0127	0.4857	0.0073	0.4938	9.93	1075	22.3
M12C-04_2-4	8.8935	0.0420	0.2867	0.0127	0.4891	0.0073	0.5073	9.89	1087	22.5
M12C-04_2-5	8.9411	0.0421	0.2870	0.0127	0.4932	0.0073	0.4885	9.93	1090	22.4
M12C-04_3-1	10.3160	0.0454	0.3178	0.0129	0.5642	0.0076	0.7428	11.42	1086	20.3
M12C-04_3-2	10.2674	0.0452	0.3242	0.0129	0.5648	0.0076	0.7427	11.39	1089	20.4
M12C-04_3-3	10.3746	0.0455	0.3264	0.0129	0.5688	0.0076	0.7428	11.50	1086	20.2
M12C-04_3-4	10.2349	0.0453	0.3076	0.0129	0.5755	0.0077	0.7681	11.30	1118	20.8
M12C-04_3-5	10.1098	0.0449	0.3137	0.0129	0.5705	0.0076	0.7459	11.20	1118	20.8
M12C-04_4-1	10.6589	0.0461	0.3135	0.0129	0.5974	0.0077	0.7368	11.75	1116	20.2
M12C-04_4-2	10.6597	0.0461	0.2919	0.0129	0.5946	0.0077	0.7392	11.67	1118	20.3
M12C-04_4-3	10.5469	0.0458	0.3048	0.0129	0.5858	0.0077	0.7347	11.60	1108	20.2
M12C-04_4-4	10.8378	0.0465	0.3104	0.0130	0.5959	0.0077	0.7344	11.91	1098	19.8
M12C-04_4-5	10.7369	0.0462	0.3131	0.0129	0.5867	0.0077	0.7259	11.82	1090	19.8

Analysis	Th [wt %]	±2σ	U [wt %]	±2σ	Pb [wt %]	±2σ	Y [wt %]	Th* [wt %]	Age [Ma]	±1σ
Unaltered; Average age ±2σ = 1074±6.7 Ma; MSWD = 0.77										
M12N-04_1-1	10.7791	0.0465	0.3255	0.0131	0.5794	0.0077	0.7640	11.90	1069	19.6
M12N-04_1-2	10.5843	0.0462	0.3201	0.0130	0.5742	0.0077	0.7256	11.69	1079	20.0
M12N-04_2-4	11.2180	0.0473	0.3199	0.0131	0.6013	0.0077	0.7114	12.32	1072	19.1
M12N-04_2-5	11.2229	0.0473	0.3347	0.0131	0.6080	0.0078	0.7245	12.38	1079	19.2
M12N-04_3-4	10.7010	0.0464	0.3176	0.0131	0.5796	0.0077	0.7374	11.80	1079	19.9
M12N-04C_1-5	11.2295	0.0957	0.3528	0.0133	0.6025	0.0076	0.9369	12.45	1064	20.8
M12N-04C_1-6	10.9688	0.0937	0.3504	0.0132	0.6011	0.0076	0.9409	12.18	1084	21.2
M12N-04C_1-7	11.0135	0.0942	0.3504	0.0133	0.6039	0.0077	0.9356	12.23	1085	21.3
M12N-04C_1-8	11.2003	0.0955	0.3489	0.0133	0.5973	0.0076	0.9212	12.40	1058	20.8
Altered										
M12N-04_2-1	3.3215	0.0268	0.0608	0.0115	0.0989	0.0057	0.1453	3.52	624	44.2
M12N-04_2-2	4.8266	0.0316	0.0817	0.0119	0.1254	0.0058	0.1902	5.10	547	30.8
M12N-04_2-3	4.5126	0.0307	0.0882	0.0117	0.1364	0.0059	0.1808	4.81	630	33.7
M12N-04_3-1	4.7766	0.0314	0.0895	0.0117	0.1295	0.0058	0.2104	5.07	568	31.1
M12N-04_3-2	4.6864	0.0312	0.1027	0.0118	0.1390	0.0059	0.2063	5.03	614	32.4
M12N-04_3-3	3.2830	0.0268	0.0529	0.0115	0.0580	0.0055	0.0876	3.46	375	41.0
M12N-04C_1-1	4.4495	0.0450	0.0368	0.0114	0.1594	0.0059	0.1826	4.57	771	38.0
M12N-04C_1-2	4.7467	0.0472	0.1101	0.0116	0.1517	0.0059	0.2568	5.11	658	33.0
M12N-04C_1-3	5.3955	0.0520	0.1379	0.0119	0.1910	0.0060	0.3431	5.86	722	30.3
M12N-04C_1-4	4.3014	0.0439	0.1036	0.0116	0.1476	0.0059	0.2202	4.65	704	36.6
Unaltered; Average age ±2σ = 1100±4.8 Ma; MSWD = 0.63										
M12C-05_1-1	10.3223	0.0454	0.3233	0.0129	0.5679	0.0076	0.8211	11.44	1090	20.3
M12C-05_1-2	10.3522	0.0455	0.3345	0.0130	0.5744	0.0077	0.8754	11.51	1096	20.3
M12C-05_1-3	10.2644	0.0453	0.3402	0.0130	0.5784	0.0077	0.8587	11.44	1110	20.5
M12C-05_1-4	10.3998	0.0457	0.3391	0.0131	0.5768	0.0077	0.8521	11.57	1094	20.2
M12C-05_1-5	10.2645	0.0453	0.3284	0.0131	0.5705	0.0077	0.8386	11.40	1099	20.6
M12C-05_2-1	10.2674	0.0452	0.3372	0.0129	0.5683	0.0076	0.8347	11.43	1091	20.3
M12C-05_2-2	10.3303	0.0455	0.3389	0.0131	0.5754	0.0077	0.8337	11.50	1098	20.4
M12C-05_2-3	10.3785	0.0455	0.3383	0.0130	0.5857	0.0077	0.8462	11.55	1113	20.5
M12C-05_2-4	10.2524	0.0453	0.3370	0.0130	0.5781	0.0077	0.8454	11.42	1111	20.6
M12C-05_3-1	8.0731	0.0401	0.2386	0.0125	0.4469	0.0071	0.3517	8.90	1102	24.6
M12C-05_3-2	8.1621	0.0403	0.2412	0.0125	0.4488	0.0071	0.3396	9.00	1095	24.1
M12C-05_3-3	8.1009	0.0401	0.2443	0.0125	0.4482	0.0071	0.3595	8.95	1100	24.4
M12C-05_3-4	8.1499	0.0403	0.2405	0.0125	0.4557	0.0071	0.3334	8.98	1113	24.4
M12C-05_3-5	8.1400	0.0401	0.2421	0.0124	0.4505	0.0071	0.3418	8.98	1102	24.2
M12C-05_4-1	10.7184	0.0463	0.3194	0.0130	0.5830	0.0077	0.7313	11.82	1083	19.8
M12C-05_4-2	10.6644	0.0461	0.3196	0.0129	0.5950	0.0077	0.7110	11.77	1109	20.1
M12C-05_4-3	10.6991	0.0461	0.3133	0.0129	0.5913	0.0077	0.7292	11.78	1102	19.9
M12C-05_4-4	10.5292	0.0458	0.3159	0.0129	0.5828	0.0077	0.7221	11.62	1101	20.1
M12C-05_4-5	10.7632	0.0463	0.3046	0.0129	0.5894	0.0077	0.7183	11.82	1095	20.0
Unaltered; Average age ±2σ = 1081±7.3 Ma; MSWD = 0.68										
M12N-05_1-4	11.2156	0.0474	0.3425	0.0132	0.6030	0.0078	0.6951	12.40	1069	19.1
M12N-05_1-5	11.0509	0.0469	0.3392	0.0131	0.5977	0.0077	0.6945	12.22	1074	19.3
M12N-05_1-6	11.0562	0.0470	0.3128	0.0131	0.5998	0.0077	0.7281	12.14	1085	19.5
M12N-05_1-7	11.0936	0.0471	0.3309	0.0131	0.6075	0.0078	0.7647	12.24	1090	19.5
M12N-05C_1-6	12.7771	0.1074	0.3919	0.0136	0.6968	0.0080	1.2010	14.13	1083	19.5
M12N-05C_1-7	12.7707	0.1073	0.3903	0.0135	0.6995	0.0080	1.2014	14.12	1088	19.5
M12N-05C_1-8	12.8111	0.1076	0.4007	0.0136	0.6951	0.0080	1.2099	14.20	1076	19.4
Altered										
M12N-05_1-1	3.2555	0.0266	0.0424	0.0114	0.0144	0.0054	0.0580	3.39	96	37.3
M12N-05_1-2	5.2426	0.0327	0.0714	0.0117	0.0617	0.0056	0.1065	5.47	253	25.3

Analysis	Th [wt %]	±2σ	U [wt %]	±2σ	Pb [wt %]	±2σ	Y [wt %]	Th* [wt %]	Age [Ma]	±1σ
M12N-05_1-3	6.8752	0.0371	0.0536	0.0117	0.0268	0.0055	0.1216	7.05	86	18.1
M12N-05C_1-1	2.9899	0.0341	0.0393	0.0113	0.0141	0.0053	0.0424	3.12	102	40.4
M12N-05C_1-2	2.6944	0.0320	0.0360	0.0113	0.0102	0.0053	0.0570	2.81	82	44.4
M12N-05C_1-3	5.1182	0.0500	0.0498	0.0115	0.0249	0.0054	0.0616	5.28	106	24.3
M12N-05C_1-4	1.8673	0.0258	0.0169	0.0111	0.0153	0.0053	0.0382	1.92	179	67.0
M12N-05C_1-5	1.8951	0.0260	0.0419	0.0111	0.0180	0.0053	0.0562	2.03	199	63.8
Unaltered; Average age ±2σ = 1088±5.0 Ma; MSWD = 1.05										
M12C-15_1-1	10.9781	0.0469	0.3266	0.0131	0.5961	0.0077	0.7320	12.11	1081	19.5
M12C-15_1-2	10.8815	0.0468	0.3322	0.0132	0.5910	0.0077	0.7398	12.03	1079	19.6
M12C-15_1-3	11.1237	0.0473	0.3250	0.0132	0.5989	0.0078	0.7286	12.25	1074	19.4
M12C-15_2-1	10.5230	0.0460	0.3344	0.0132	0.5758	0.0077	0.7909	11.68	1083	20.1
M12C-15_2-2	10.6636	0.0463	0.3246	0.0132	0.5770	0.0077	0.8327	11.79	1076	19.9
M12C-15_1-1	10.9211	0.0933	0.3074	0.0129	0.6048	0.0076	0.7028	11.99	1107	21.7
M12C-15_1-2	10.7561	0.0921	0.4018	0.0127	0.5925	0.0075	0.6450	12.14	1072	20.9
M12C-15_1-3	10.7703	0.0923	0.4262	0.0126	0.6064	0.0077	0.5847	12.25	1088	21.0
M12C-15_2-1	8.2802	0.0737	0.2668	0.0126	0.4546	0.0071	0.3927	9.20	1085	25.5
M12C-15_2-2	8.2839	0.0737	0.2575	0.0126	0.4642	0.0071	0.3947	9.18	1110	25.8
M12C-15_2-3	8.3670	0.0743	0.2494	0.0126	0.4659	0.0071	0.3981	9.23	1108	25.7
M12C-15_3-1	10.5061	0.0904	0.4008	0.0129	0.5917	0.0076	0.8822	11.89	1093	21.5
M12C-15_3-3	10.5913	0.0911	0.3200	0.0131	0.5868	0.0076	0.8753	11.70	1101	22.1
M12C-15_4-1	9.5618	0.0833	0.2753	0.0127	0.5185	0.0073	0.6174	10.51	1083	23.3
M12C-15_4-2	9.3733	0.0818	0.2793	0.0127	0.5163	0.0073	0.6153	10.34	1096	23.6
M12C-15_4-3	9.4190	0.0822	0.2782	0.0127	0.5162	0.0073	0.6252	10.38	1092	23.7
M12C-15_5-1	10.4504	0.0899	0.3172	0.0131	0.5723	0.0075	0.8680	11.55	1088	22.1
M12C-15_5-2	10.3932	0.0895	0.3304	0.0131	0.5753	0.0075	0.8549	11.54	1095	22.1
M12C-15_5-3	10.3433	0.0891	0.3093	0.0129	0.5632	0.0075	0.8365	11.41	1084	22.1
M12C-15_5-2	10.3932	0.0895	0.3304	0.0131	0.5753	0.0075	0.8549	11.54	1095	22.1
M12C-15_5-3	10.3433	0.0891	0.3093	0.0129	0.5632	0.0075	0.8365	11.41	1084	22.1
Unaltered; Average age ±2σ = 1084±7.9 Ma; MSWD = 1.89										
M12N-15_1-2	8.8713	0.0421	0.2730	0.0127	0.4799	0.0073	1.1476	9.81	1074	22.6
M12N-15_1-3	8.7326	0.0419	0.2633	0.0127	0.4697	0.0073	1.1600	9.64	1070	22.9
M12N-15_2-5	8.6165	0.0415	0.2749	0.0128	0.4829	0.0073	0.3962	9.57	1108	23.4
M12N-15_2-6	8.5621	0.0413	0.2795	0.0127	0.4830	0.0073	0.3985	9.53	1112	23.4
M12N-15C_2-5	8.6945	0.0768	0.2697	0.0127	0.4666	0.0071	0.5164	9.63	1065	24.5
M12N-15C_2-6	8.7279	0.0771	0.2660	0.0127	0.4768	0.0071	0.5245	9.65	1085	24.7
M12N-15C_2-7	8.8968	0.0783	0.2844	0.0128	0.4831	0.0071	0.4128	9.88	1074	24.1
M12N-15C_2-8	8.7597	0.0773	0.2793	0.0127	0.4804	0.0071	0.4196	9.73	1085	24.5
M12N-15C_2-9	8.7879	0.0775	0.2779	0.0127	0.4812	0.0071	0.4068	9.75	1084	24.5
Altered										
M12N-15_1-1	3.1034	0.0263	0.0350	0.0114	0.0165	0.0053	0.0665	3.22	116	39.1
M12N-15_2-1	4.0639	0.0293	0.0659	0.0116	0.0677	0.0055	0.0883	4.28	354	33.0
M12N-15_2-2	3.6300	0.0279	0.0428	0.0115	0.0431	0.0055	0.0697	3.77	256	35.9
M12N-15_2-3	4.8154	0.0315	0.0885	0.0117	0.1461	0.0058	0.1425	5.11	635	31.5
M12N-15_2-4	4.1750	0.0297	0.0625	0.0117	0.0841	0.0057	0.1063	4.38	428	33.8
M12N-15C_1-1	2.9319	0.0336	0.0300	0.0112	0.0179	0.0053	0.0677	3.03	133	42.0
M12N-15C_2-1	1.3111	0.0217	0.0229	0.0111	0.0059	0.0053	0.0618	1.38	95	89.4
M12N-15C_2-2	2.1793	0.0281	0.0303	0.0112	0.0157	0.0053	0.0499	2.28	155	56.2
M12N-15C_2-3	3.2051	0.0357	0.0529	0.0113	0.0732	0.0055	0.1215	3.38	483	44.0
M12N-15C_2-4	3.3722	0.0370	0.0467	0.0113	0.0467	0.0055	0.0942	3.52	297	39.3
Burnet monazite; Average age ±2σ = 1072±2.8 Ma; MSWD = 1.89										
MX-12SM_1-1	9.0852	0.0426	0.2961	0.0129	0.4895	0.0073	0.5196	10.11	1064	22.1
MX-12SM_1-2	9.1033	0.0426	0.2864	0.0129	0.4856	0.0073	0.4937	10.09	1058	22.0

Analysis	Th [wt %]	±2σ	U [wt %]	±2σ	Pb [wt %]	±2σ	Y [wt %]	Th* [wt %]	Age [Ma]	±1σ
MX-12SM_1-3	9.0960	0.0429	0.2878	0.0129	0.4922	0.0074	0.5200	10.09	1072	22.4
MX-12SM_1-4	9.1297	0.0428	0.2906	0.0129	0.4840	0.0073	0.5108	10.13	1050	22.0
MX-12SM_1-5	8.9866	0.0423	0.2827	0.0128	0.4787	0.0073	0.5100	9.96	1056	22.2
MX-12SM_1-6	9.0441	0.0425	0.2983	0.0129	0.4813	0.0073	0.5049	10.07	1050	22.1
MX-12SM_1-7	9.1058	0.0421	0.2886	0.0127	0.4920	0.0073	0.5099	10.10	1070	21.9
MX-12SM_2-1	9.4617	0.0430	0.2944	0.0128	0.5104	0.0073	0.6375	10.48	1070	21.3
MX-12SM_2-2	9.5737	0.0435	0.3045	0.0129	0.5191	0.0075	0.6169	10.63	1073	21.4
MX-12SM_2-3	9.5058	0.0435	0.2958	0.0129	0.5135	0.0075	0.6158	10.53	1072	21.6
MX-12SM_2-4	9.4199	0.0436	0.2938	0.0129	0.5126	0.0075	0.6431	10.44	1079	21.8
MX-12SM_2-5	9.5577	0.0439	0.3050	0.0129	0.5191	0.0075	0.6219	10.61	1075	21.5
MX-12SM_2-6	9.5268	0.0438	0.3073	0.0130	0.5127	0.0075	0.6236	10.59	1064	21.5
MX-12SM_3-1	9.0498	0.0427	0.2786	0.0129	0.4886	0.0073	0.5272	10.01	1072	22.4
MX-12SM_3-2	8.9896	0.0425	0.2871	0.0129	0.4876	0.0073	0.5120	9.98	1073	22.4
MX-12SM_3-3	8.9779	0.0423	0.2865	0.0127	0.4793	0.0073	0.5026	9.97	1057	22.2
MX-12SM_3-4	9.0614	0.0426	0.2822	0.0129	0.4854	0.0073	0.5317	10.04	1063	22.3
MX-12SM_3-5	8.9357	0.0423	0.2925	0.0128	0.4832	0.0073	0.5042	9.95	1067	22.4
MX-12SM_3-6	9.0728	0.0426	0.2983	0.0128	0.4964	0.0073	0.5058	10.10	1079	22.2
MX-12SM_4-1	11.1243	0.0473	0.3267	0.0132	0.6038	0.0079	0.7830	12.25	1082	19.5
MX-12SM_4-2	11.1909	0.0469	0.3301	0.0130	0.5990	0.0077	0.7968	12.33	1067	19.0
MX-12SM_4-3	11.1015	0.0466	0.3388	0.0130	0.5983	0.0077	0.7955	12.27	1071	19.1
MX-12SM_4-4	10.9403	0.0462	0.3326	0.0129	0.5849	0.0077	0.8133	12.09	1063	19.2
MX-12SM_4-5	11.1425	0.0472	0.3409	0.0131	0.5885	0.0077	0.7810	12.32	1050	19.0
MX-12SM_4-6	11.0763	0.0471	0.3325	0.0131	0.5917	0.0078	0.7758	12.22	1064	19.3
MX-12SM_5-1	14.8997	0.0551	0.4608	0.0140	0.7964	0.0087	1.2926	16.49	1061	15.9
MX-12SM_5-2	14.5576	0.0545	0.4555	0.0139	0.7970	0.0087	1.2307	16.13	1085	16.3
MX-12SM_5-3	14.3424	0.0543	0.4397	0.0139	0.7924	0.0087	1.2199	15.87	1097	16.6
MX-12SM_5-4	14.2808	0.0541	0.4504	0.0139	0.7816	0.0086	1.2333	15.84	1084	16.5
MX-12SM_5-5	14.3494	0.0542	0.4500	0.0139	0.7906	0.0087	1.2467	15.91	1091	16.5
MX-12SM_5-6	14.4524	0.0543	0.4222	0.0138	0.7840	0.0087	1.2459	15.91	1082	16.5
MX-12SM_6-1	11.4614	0.0481	0.3704	0.0134	0.6164	0.0079	0.9078	12.74	1063	18.9
MX-12SM_6-2	11.2802	0.0477	0.3655	0.0133	0.6107	0.0079	0.9075	12.54	1070	19.1
MX-12SM_6-3	11.2067	0.0475	0.3562	0.0133	0.6022	0.0079	0.9110	12.44	1064	19.2
MX-12SM_6-4	11.4488	0.0480	0.3937	0.0134	0.6170	0.0079	0.9365	12.81	1059	18.8
MX-12SM_6-5	11.4426	0.0479	0.3723	0.0133	0.6226	0.0079	0.9138	12.73	1075	18.9
MX-12SM_6-6	11.4669	0.0474	0.3776	0.0131	0.6141	0.0078	0.9038	12.77	1057	18.5
MX-12SM_7-1	8.2589	0.0407	0.2409	0.0126	0.4470	0.0071	0.3600	9.09	1080	24.0
MX-12SM_7-2	8.2650	0.0405	0.2555	0.0126	0.4480	0.0071	0.3561	9.15	1076	23.8
MX-12SM_7-3	8.2872	0.0406	0.2559	0.0127	0.4488	0.0071	0.3544	9.17	1075	23.8
MX-12SM_7-4	8.3101	0.0402	0.2573	0.0125	0.4449	0.0070	0.3573	9.20	1063	23.2
MX-12SM_7-5	8.3099	0.0407	0.2402	0.0126	0.4462	0.0071	0.3702	9.14	1072	23.8
MX-12SM_7-6	8.2886	0.0407	0.2477	0.0126	0.4491	0.0071	0.3712	9.14	1079	23.8
BrtMnz-2	10.6912	0.0463	0.3515	0.0132	0.5825	0.0077	0.8676	11.91	1075	19.8
BrtMnz-3	10.6000	0.0460	0.3434	0.0131	0.5724	0.0077	0.8421	11.79	1067	19.8
BrtMnz-4	10.8079	0.0465	0.3509	0.0132	0.5875	0.0077	0.8702	12.02	1074	19.6
BrtMnz-5	10.5602	0.0459	0.3224	0.0130	0.5730	0.0077	0.8091	11.67	1078	20.0
BrtMnz-6	10.4798	0.0457	0.3283	0.0131	0.5673	0.0077	0.7944	11.61	1073	20.1
BrtMnz-7	10.3819	0.0458	0.3376	0.0131	0.5614	0.0077	0.7601	11.55	1068	20.2
BrtMnz-8	10.2777	0.0453	0.3186	0.0130	0.5607	0.0076	0.7907	11.38	1082	20.4
BrtMnz-9	10.1626	0.0453	0.3230	0.0131	0.5571	0.0077	0.7735	11.28	1085	20.7
BrtMnz-10	10.1576	0.0451	0.3357	0.0131	0.5627	0.0077	0.7841	11.32	1092	20.7
BrtMnz-11	10.0710	0.0450	0.3432	0.0125	0.5497	0.0076	0.6973	11.26	1073	20.4